LABORATORI NAZIONALI DI FRASCATI
SIS-Pubblicazioni

LNF-97/033 (IR)
16 Settembre 1997

STATUS OF THE KLOE EXPERIMENT

The KLOE Collaboration

Abstract

The present status of the KLOE Experiment is presented in this collection of recent KLOE notes.

PACS:11.30.Er,13.20.Eb;13.20Jf;29.40.Gx;29.40.Vj

Paper submitted to the
XVIII International Symposium on Lepton Photon Interactions,
Hamburg Germany, July 28, August 1, 1997

M. Adinolfi[m], A. Aloisio[g], A. Andryakov[c], A. Angeletti[k], A. Antonelli[c], C. Bacci[n], R. Baldini-Ferroli[c], G. Barbiellini[r], G. Bencivenni[c], S. Bertolucci[c], C. Bini[k], C. Bloise[c], V. Bocci[m], F. Bossi[c], P. Branchini[o], L. Bucci[k], G. Cabibbo[c], A. Calcaterra[c], R. Caloi[k], P. Campana[c], G. Capon[c], G. Carboni[m], M. Carboni[c], C. Carusotti[c], G. Cataldi[d], F. Ceradini[n], F. Cervelli[j], F. Cevenini[g], G. Chiefari[g], P. Ciambrone[c], I. Cohen[q], C. Colantuono[c], S. Conetti[s], S. Conticelli[c], G. Corti[s], E. De Lucia[k], R. De Sangro[c], P. De Simone[c], G. De Zorzi[k], S. Dell'Agnello[c], A. Denig[d], A. Di Benedetto[c], G. Di Cosimo[k], A. Di Domenico[k], S. Di Falco[j], A. Doria[g], F. Donno[c], E. Drago[g], V. Elia[e], L. Entesano[r], O. Erriquez[a], A. Farilla[a], F. M. Favero[c], G. Felici[c], A. Ferrari[k], M. L. Ferrer[c], G. Finocchiaro[c], D. Fiore[g], C. Forti[c], G. Foti[r], A. Franceschi[c], P. Franzini[k,i], A. Galli[k], M. L. Gao[c,b], C. Gatto[g], P. Gauzzi[k], S. Giovannella[c], V. Golovatyuk[e], E. Gorini[e], F. Grancagnolo[e], W. Grandegger[c], E. Graziani[o], P. Guarnaccia[a], U. v. Hagel[d], H. G. Han[c,b], S. W. Han[c,b], M. Incagli[j], L. Ingrosso[c], W. Kim[c], W. Kluge[d], V. Kulikov[f], F. Lacava[k], G. Lanfranchi[k], J. Lee-Franzini[c,p], T. Lomtadze[j], C. Luisi[k], A. Martini[c], M. M. Massai[j], W. Mei[c], L. Merola[g], R. Messi[m], S. Miscetti[c], A. Moalem[h], S. Moccia[c], F. Murtas[c], M. Napolitano[g], A. Nedosekin[f], G. F. Palamà[e], M. Panareo[e], L. Paoluzi[m], E. Pasqualucci[c], L. Passalacqua[c], M. Passaseo[k], A. Passeri[o], V. Patera[l,c], E. Petrolo[k], G. Petrucci[c], D. Picca[k], M. Piccolo[c], A. Pintus[c], G. Pirozzi[g], L. Pontecorvo[k], M. Primavera[e], F. Ruggieri[a], E. Santovetti[m], G. Saracino[g], R. D. Schamberger[p], C. Schwick[j], A. Sciubba[l,c], F. Scuri[r], I. Sfiligoi[r], S. Spagnolo[e], E. Spiriti[o], C. Stanescu[o], L. Tortora[o], E. Valente[k], P. Valente[m], G. Venanzoni[j], S. Veneziano[k], D. Vettoretti[c], S. Weseler[d], Y. G. Xie[c,b], C. D. Zhang[b], J. Q. Zhang[b], P. P. Zhao[c,b],

[a] Dipartimento di Fisica dell'Università e Sezione INFN, Bari, Italy.
[b] Institute of High Energy Physics of Academica Sinica, Beijing, China.
[c] Laboratori Nazionali di Frascati dell'INFN, Frascati, Italy.
[d] Institut für Experimentelle Kernphysik, Universität Karlsruhe, Germany.
[e] Dipartimento di Fisica dell'Università e Sezione INFN, Lecce, Italy.
[f] Institute for Theoretical and Experimental Physics, Moscow, Russia.
[g] Dipartimento di Scienze Fisiche dell'Università e Sezione INFN, Napoli, Italy.
[h] Physics Department, Ben-Gurion University of the Negev, Israel.
[i] Physics Department, Columbia University, New York, USA.
[j] Dipartimento di Fisica dell'Università e Sezione INFN, Pisa, Italy.
[k] Dipartimento di Fisica dell'Università, La Sapienza e Sezione INFN di Roma, Roma, Italy.
[l] Dipartimento di Energetica dell'Università, La Sapienza Roma , Italy.
[m] Dipartimento di Fisica dell'Università, Tor Vergata e Sezione INFN di Roma II, Roma, Italy.
[n] Dipartimento di Fisica dell'Università di Roma Tre e Sezione INFN di Roma, Roma, Italy.
[o] Istituto Superiore di Sanità and Sezione INFN, ISS, Roma, Italy.
[p] Physics Department, State University of New York at Stony Brook, USA.
[q] School of Physics and Astronomy, Tel Aviv, Israel.
[r] Dipartimento di Fisica dell'Università e Sezione INFN, Trieste/Udine, Italy.
[s] Physics Department, University of Virginia, USA.

1 Introduction

The KLOE detector, at present under construction for operations at the Frascati ϕ-factory DAΦNE, is a general purpose detector whose major aim is the study of direct CP violation in the neutral kaon system. Its ultimate goal is to reach an accuracy of $O(10^{-4})$ in the measurement of the parameter Re(ϵ'/ϵ). KLOE will be also capable of doing a whole spectrum of other measurements, such as tests of CPT in K decays, studies of chiral perturbation theory and detailed light hadron spectroscopy.

The accelerator complex consists of a superconducting LINAC, which accelerates electrons and positrons to 510 MeV, followed by an Accumulator Ring, which provides up to 120 bunches of each type of particles to the two separate Main Rings intersecting in two regions only. The first collisions are expected for September 1997. The design peak luminosity is 10^{33} cm^{-2}s^{-1} , which corresponds to a ϕ production rate of 5 kHz.

The detector consists of a cylindrical drift chamber surrounded by a lead-scintillating fibres electromagnetic calorimeter. Moreover, two small calorimeters cover the quadrupoles of the low-β insertion which are located inside the detector. It operates in an axial magnetic field of 0.6 T provided by a 2.5 m radius superconducting solenoid.

The design of the drift chamber was driven by the following considerations:

- It has to maximize the homogeneity and isotropy of the active tracking volume, because of the long decay path of the K_L and the isotropic angular distribution of the charged products
- It has to achieve a high efficiency for the reconstruction of the K_L decay to two charged pions
- It has to optimize resolution at low momentum values
- It has to minimize the number of wires, to minimize multiple scattering and maintain the electronics channels count within reasonable limits.

This has resulted in a 3.2 m long, 2 m radius, cylindrical chamber, with carbon fibre plates and all-stereo cell geometry. Its stringing started in November 1996 and is proceeding regularly towards its end, expected for November 1997. In total, more than 52000 wires, both sense and field ones, will be strung.

Reconstruction of the $\pi^0\pi^0$ decay mode of the K_L, the determination of its decay point and the efficient rejection of the more abundant three π^0's background are the main requirements which have determined the design of the electromagnetic calorimeter. It consists of lead grooved foils, interleaved with layers of scintillating fibres, for a total thickness of 23 cm, corresponding to about 15 radiation lengths. The calorimeter is organized in 24 barrel modules, 4.3 m long, and 64 C-shaped endcap modules with lengths ranging from 1.5 to 4.5 m.

Particularly relevant is the time resolution on photons, which has been proven to behave as $\sigma_t = 52$ ps $/\sqrt{E}$, with E in GeV.

All the calorimeter's modules have been built, and will be assembled together in November 1997, inside the coil, after the complete mapping of the latter will be finished.

The quadrupoles of the low-β insertion, being located inside the detector, can lead to losses of photons from $K_L \to \pi^0\pi^0\pi^0$ decays, a very dangerous background for CP violation studies. In order to minimize this effect, a special electromagnetic calorimeter (QCAL) surrounding the focalization quadrupoles has also been designed.

The expected data rates together with the very high sensitivity required in the control of all possible systematic effects make the requirements on the trigger and data acquisition system a real challenge in the field. Inefficiencies and error rates must be minimized to insure that no biases are introduced at these levels. Particular care must be taken in order to insure that the channels involved in the measurement of the CP violating parameters are triggered and acquired with very high and equal efficiencies.

This is possible thanks to a very flexible trigger system, and a custom-designed DAQ system which allows us to handle data throughput as high as 50 MBytes/s. The status of FEE, DAQ and Trigger systems is well advanced, and everything is expected to be ready for the detector's roll-in, in Spring 1998.

A more detailed discussion of the present status of the various detector's components can be found in the attached notes, listed in the following:

- Quality checks and first calibration of the KLOE e.m. Calorimeter
- The ADC and TDC of the KLOE e.m. Calorimeter
- The construction of the KLOE Drift Chamber: present status
- Electrostatic digital method of wire tension measurement for the KLOE Drift Chamber
- Results for the full length prototype of the KLOE Drift Chamber
- dE/dx measurement in a He-based gas mixture
- Performances of a multichannel 1 Ghz TDC ASIC for the KLOE Tracking Chamber
- The Trigger and Data Acquisition System of the KLOE Experiment
- Message system and data transmission in the KLOE DAQ System
- Readout optimization for the KLOE QCAL tile calorimeter

Quality Checks and First Calibration of the KLOE e.m. Calorimeter [†]

Abstract

The construction of the KLOE lead-scintillating fibres electromagnetic calorimeter has been completed. The final results of the extensive quality checks of all the KLOE calorimeter modules are presented here. The measurements have been done at the Frascati Laboratories with a cosmic ray test facility using minimum ionizing particles. The results show that all the calorimeter modules are within the design specifications in order to get the time and the energy resolutions for its operation in the KLOE experiment. Moreover all the calorimeter elements have been calibrated using minimum ionizing particles.

1 The KLOE electromagnetic calorimeter

The KLOE electromagnetic calorimeter is a fine sampling lead-scintillating fibres calorimeter [1)]. It consists of lead grooved foils 0.5 mm thick intervealed with layers of 1 mm diameter scintillating fibres glued by means of an epoxy resin. The lead-fibre-glue volume composition is 42:48:10. Every module has a thickness of 23 cm, corresponding to about 15 radiation lengths [2)].

The calorimeter consists of 24 barrel modules 4.3 m long, and of 64 C-shaped endcap modules with lengths, ranging from 1.5 up to 4.5 m. Every module is segmented in read-out elements of $\sim 4 \times 4\ cm^2$ and the light is read-out through plexiglass light guides and fine-mesh photomultipliers [3)] on both sides of every element. The total number of channels is 4880. Two kinds of scintillating fibres have been employed [4)]: Kuraray SCSF-81 in the inner half of the calorimeter and Pol.Hi.Tech. 0046 in the outer half.

2 Quality checks

The Cosmic Ray Test Stand is a cosmic ray telescope based on 4 layers of streamer tubes, 12 scintillators and 1 fibre counter. It provides an external trigger and allows to reconstruct the cosmic ray tracks and their impact positions on the calorimeter modules under test [5)]. The set-up allows to test up to 4 modules with different geometries at the same time.

ADC and TDC spectra are obtained for every read-out element. The following quantities are measured: from the ADC spectra the mip peak at half of the module length (mip in the following), the attenuation length λ, and the average number of photoelectrons $N_{p.e.}$; form the TDC spectra, the light velocity in the fibres, the time resolution and the resolution in the coordinate along the fibres that is obtained by the time difference between the two sides.

Fig.2 shows the average attenuation length and the average number of photoelectrons at

[†] *Contributed paper to the VII Pisa Meeting on Advanced Detectors, Elba Italy, May 25-31, 1997*

the module centre as a function of the module number for the barrel modules and as a function of the fibre length for the endcap modules. The barrel module number ranges from 0 to 24. Module 0 is the first full-size prototype built in 1994 and tested on beam at P.S.I. [6]; modules form 1 to 24 are the modules that we'll use in the KLOE experiment. The results are shown separately for the inner and the outer hlves of the calorimeter.

For the endcap modules the fibre length is the relevant parameter that determines the

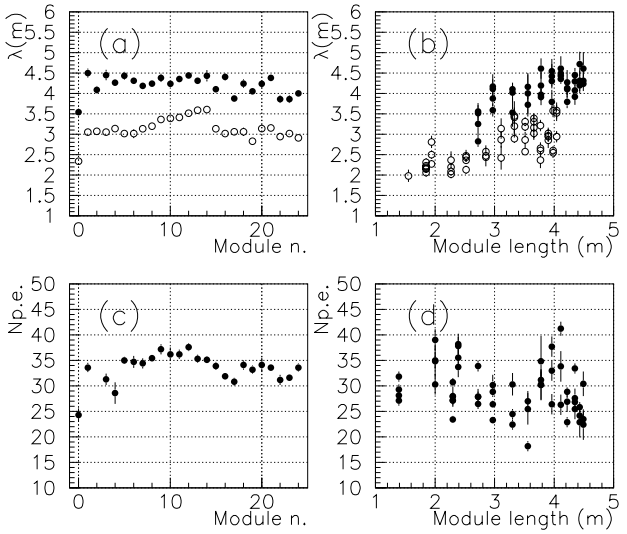

Figure 1: Summary of the measured performancies of the KLOE calorimeter modules. (a) Attenuation length as a function of the module number for the barrel modules; inner part (full circles) and outer part of the calorimeter (open circles). (b) Attenuation length as a function of the fibre length for the endcap modules. (c) Average number of photoelectrons as a function of the module number for the inner part of the barrel modules and (d) as a function of the fibre length for the inner part of the endcap modules.

performance. Infact the shorter is the fibre length, the larger is the expected light yield for particles impinging at half of the module length. In order to have homogeneous performance, the short modules have been equipped with the worst quality fibrs and the lower quantum efficiency photomultipliers.

The light yield at half of the module length of barrel and endcap modules is almost homogeneous all over the calorimeter. The endcap modules are characterized by a slightly lower average and by larger fluctuations.

The quality of the barrel modules improves respect to the module 0 in terms of light yield and attenuation length. This is due to the improved quality of the fibres and to the special care devoted to handle the scintillating fibres , as they resulted to be damaged by the ultraviolet component of natural and artificial light [7]. Taking into account that the energy

release of a mip in an element corresponds to the energy release of a 32 MeV photon in the calorimeter [6], we extrapolate a slight improvement concerning the energy resolution that is dominated by the sampling fluctuations, and a large improvement for the time resolution that is dominated by the photoelectron statistics term. The expected resolutions are: $\sigma(E)/E = 4.7\%/\sqrt{E(GeV)}$ and $\sigma_t = 52ps/\sqrt{E(GeV)}$

3 Calibration

Minimum ionizing particles crossing the calorimeter elements have been used also to obtain a first step calorimeter calibration, by equalizing the charge response of all the elements. The adopted procedure is an iterative one. The mips of all the elements are measured; then the high voltage of every photomultiplier is changed according to the $HV_1 = HV_0(Q_{eq}/mip)^{1/\gamma}$ where Q_{eq} is the equalization charge, and $\gamma \sim 7.2$ is the parameter of the gain-voltage curve; then the mips are measured again. The procedure is repeated until when all the mips are within $\pm 4\%$ that is the measurement accuracy. Fig.3 shows the mip distribution for all the 2880 barrel elements in the three subsequesnt steps: the widths of the three distributions are $\sim 30\%$ at the step 0, $\sim 8\%$ after the first step and $\sim 4\%$ after the second and last one. A similar behaviour is obtained for the endcap elements.

References

1. A. Antonelli et al., Nucl. Instr. and Meth. A354 (1995) 352;
2. M. Anelli et al., KLOE Memo 97-87, 04/97;
3. A. Antonelli et al., Nucl. Instr. and Meth. A368 (1996) 628;
4. A. Antonelli et al., Nucl. Instr. and Meth. A370 (1996) 367;
5. C. Bini et al., KLOE Note 154, 01/96;
   P.Gauzzi et al., Proceed. of the 6th Internat. Conference on Calorimetry in High Energy Physics 1996, p.359;
6. A. Antonelli et al,. KLOE Note 152 10/95;
7. M. Anelli et al., KLOE Note 136, 01/95;

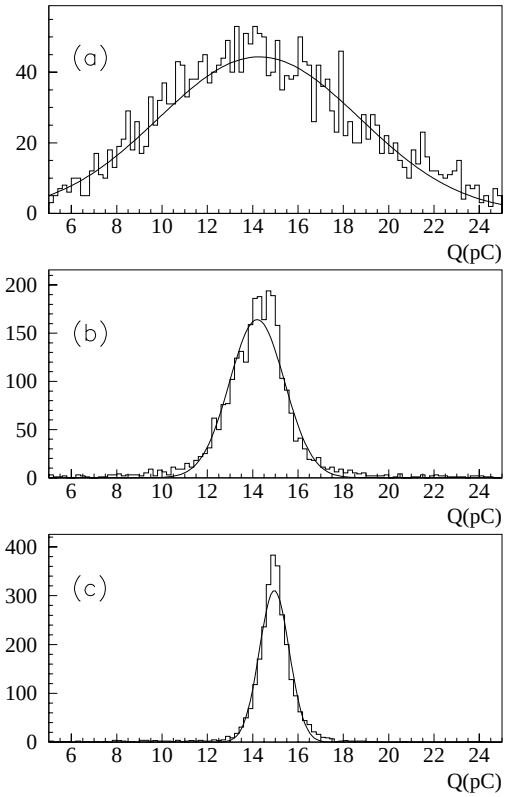

Figure 2: Result of the equalization procedure for all the barrel elements (2880 channels). (a) Mip distribution after step 0, (b) after step 1 and (c) after step 2. Q_{eq} is fixed at $15\ pC$.

The ADCs and TDCs for the KLOE Electromagnetic Calorimeter [†]

Abstract

The KLOE electromagnetic calorimeter processes signals arriving over an interval of ≈ 200 ns before the trigger time. The KLOE ADC is based on two continously analog baseline subtraction systems. A high stability monostable circuit is used at the input of the TDC operating in common start mode.

1 Introduction

The KLOE electromagnetic calorimeter (EmC) [1)] provides the position, time of arrival and energy for every particle reaching it by measuring charge and time of all read out elements. To face the arrival time spread of the same event particles at the calorimeter (≈ 200 ns) [2)], due to the small center of mass energy (1 GeV), and to avoid delaying signals, we developed, in collaboration with CAEN company, special circuits to measure charge and time.

[†] *Contributed paper to the VII Pisa Meeting on Advanced Detectors, Elba Italy, May 25-31, 1997*

2 ADC working principle and performance

The main parameters defining the KLOE ADC are: a maximum detected signal of $\approx$ 1000 photoelectrons and an arrival time window of 200 ns starting 350 ns before the trigger. The 12 bit digitizing devices, chosen for uniformity with the TDC, provide an adeguate resolution of $\approx$0.25 photoelectrons/count.

The chosen solution is based on a processing in three stages: an always open charge integrator with the desired sensitivity and a long decay time, a double analog baseline subtraction system plus a final commercial 12 bits, 1 μs conversion time monolithic ADC[‡] chip.

In fig. 3 is sketched the KLOE ADC sampling scheme. The two clocks drive the

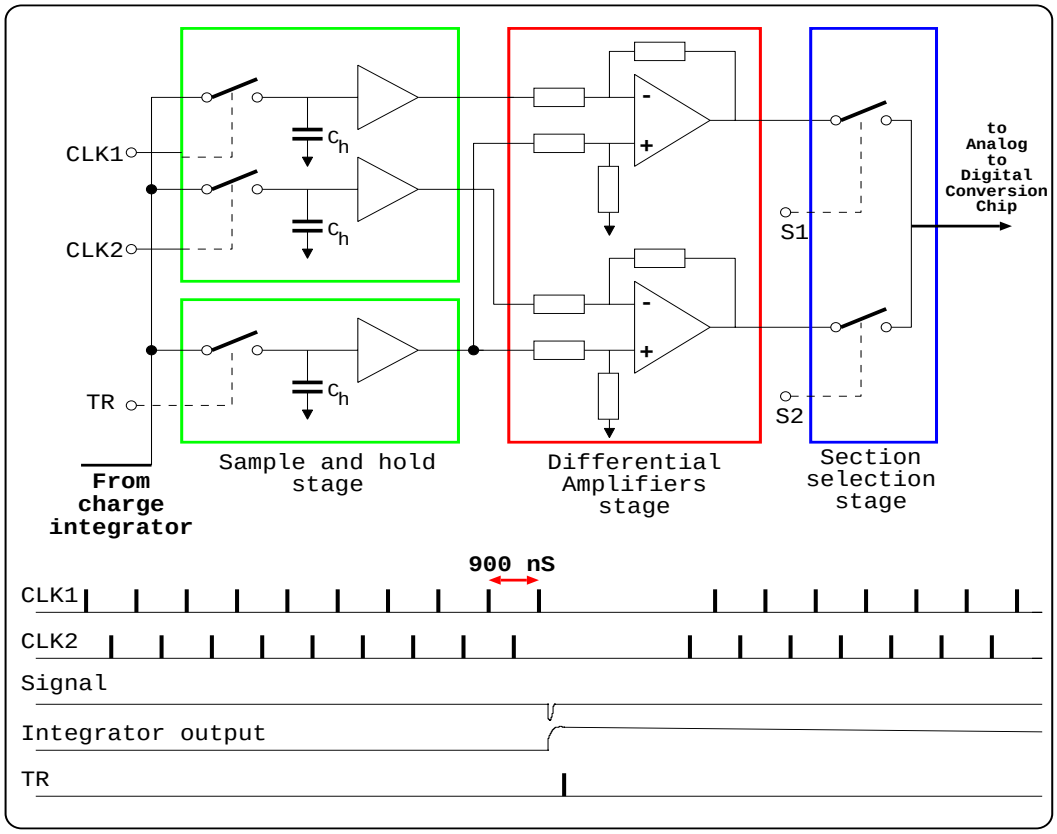

Figure 3: ADC sampling scheme

baseline S&H stages, while the TR signal related to the fast trigger T1 starts the signal sampling. A time separation from the pulse of one clock to the other clock following pulse (400 ns) longer than the 350 ns maximum delay of the trigger from the signal, allows to have the rigth baseline value stored in at least one of the two S&Hs. Then, after an analog subtraction, the logic decides via the S1, S2 signals which baseline value is used.

The spread in the arrival time of the trigger versus the signal results in the integrator

[‡]Model AD 7886, supplied by Analog Devices Company.

output to be sampled at different point of its decay tail. A very long decay time of ≈ 0.5 ms for the charge integrator is used to reduce the sampling error to the required resolution and does not produce pile up problems due to the average occupancy per channel of ≈ 100 Hz. To obtain such a decay time we used large coupling capacitors among the different stages: photomultiplier, splitter and ADC, and a double stage ADC input, formed by a voltage to current converter and a classical cascode based charge integrator [3]. The measured performance on ≈3000 channels are a pedestal RMS spread better than 1 count, an integral non linearity of less than 0.3% of full scale and a spread of the pedestal value and gain coefficient of ± 3 %.

3 TDC working principle and performance

The main constrain for the TDC is to maintain the timing resolution of the EmC [4], it must have also excellent performances with respect to resolution, linearity and stability. The dynamic range is 220 ns and the arrival time window starts 220 ns before the trigger, a 12 bit digitization chip implies a resolution of 55 ps. The different position of the signal acceptance time window from the ADC is compensated by shorter signal cables.

Each TDC channel is built around a monolithic Time-to-Analog Converter (TAC)

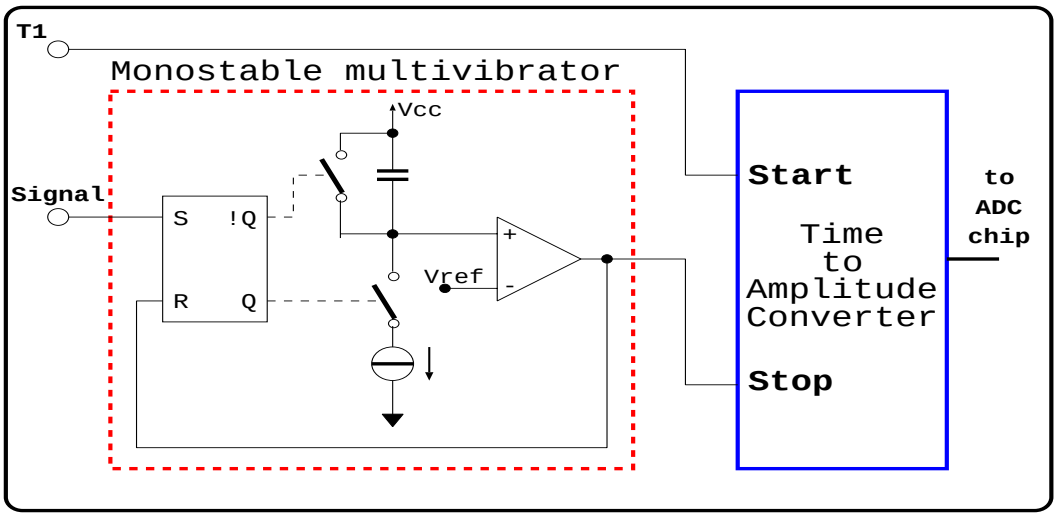

Figure 4: TDC analog input section

developed in bipolar technology, preceded by a delay circuit and followed by the same analog to digital conversion chip used in the ADC, fig. 4. The KLOE TDC works in *common start* mode, the start is provided by the fast trigger signal T1 and the stops are provided by the KLOE discriminators [5] output. The fast trigger T1, which starts the TAC conversion, is synchronized with the bunch crossing time and arrives 200-300 ns after the collision time at a rate of $\sim$ 20 kHz [2]. In order to compensate for the delay of T1, the stop signals are delayed by a monostable multivibrator at the input of each channel. Every trigger starts the conversion process and, if no stop arrives, the TAC overflows.

In this case the internal logic resets it to a pedestal value and the overflow condition is signalled in the data words.

The KLOE EmC TDC temperature dependence has been shown to be the same for all channels on a board. A single temperature compensation circuit [6], trimmered at production stage, for the whole board is used.

The measured performance on ≈ 3000 channels are a pedestal RMS spread less than 1 count, an integral non linearity of less than 0.2 % of full scale and a temperature stability better than $\pm$0.3 count/^{o}C.

4 ADC/TDC auxiliary (DAQ related) functions

The KLOE ADC and TDC are implemented on a 9U, 400 mm deep board using the VME standard bus (Caen mod. VX559/VX569). The digitizing part is housed on 30 daughter boards for the ADC and 15 daughter boards for the TDC with respectively one or two analog channel each. The digital processing section, common to ADC and TDC, starts after the voltage to digital conversion chip and is placed on the mother board itself; it includes: the latches to store one event after the ADC conversion, the zero suppression mechanism, the pedestal automatic subtraction system, a multi event FIFO (17 events deep) plus the control logic for the AXBUS interface [7], the VME standard interface and the trigger and analog part control logic.

The trigger system [2] produces two signals. The first (T1) is prompt and drives the digitizing operation that stores data on the latches after a 2 μs fixed dead time. The second (T2) drives the digital processing section; it starts the scan of the latches then passing the data to the zero suppression and pedestal subtracting logic and finally stores the results in a FIFO.

The FIFO consist of two parts.The header FIFO stores the trigger number (12 bits) plus the number of channel data surviving the zero suppression (5 bits to encode 30 channels). The data FIFO, contains the data words that includes: 12 bits of digitized data, 1 bit to indicate for the ADC the baseline used and the overflow condition for the TDC, plus a 5 bits encoded channel number. The FIFOs are readout throught the KLOE synchronous AUXBUS [7] which implements a sparse data scan mechanism and a trigger counter check to control overall synchronization.

References

1. *The KLOE Detector - Technical Proposal*, The KLOE Collaboration, LNF 93/01.
2. *The KLOE Trigger System, Addendum to the Technical Proposal*, The KLOE Collaboration, LNF 96/43.
3. P. Franzini, E. Spiriti *The ADC for the KLOE Electromagnetic Calorimeter* KLOE memo no. 94/97
4. S. Wőlfe, *Module Zero, Analysis of the 1994 Test Beam at PSI*, Kloe Note no. 134, (1995).

5. M. Anelli et al., *Tests of a Constant Fraction Discriminator for the use with the KLOE EmC,* Kloe Memo 14, (1995).
6. P. Franzini, A. Balla, P. Ciambrone, G. Corradi, G. Lanfranchi, M. Santoni *A solution for the temperature dependence compensation of the monostable multivibrator of the KLOE EmC TDC* KLOE Memo no. 52/96
7. A. Aloisio et., *A fast readout system for KLOE,* Kloe note no. 88 (jan.94).

The Construction of the KLOE Drift Chamber: Present Status [†]

Abstract

The status of the construction of the KLOE Drift Chamber is reviewed. With its 4 m diameter, it will be the biggest drift chamber ever built. The stringing of 52,000 wires is a titanic effort: details are given on the semiautomatic system, on the quality tests on wires and on the monitoring of end-plates deformations.

1 Introduction

The unconventional characteristics of the chamber are dictated by the physics demands of the KLOE experiment [1)]:

- the big size, 4 m diameter, $\simeq$ 3.3 m length, is driven by the large decay path of the K_L: λ_L = 3.43 m;
- the omogeneous and uniform packing of the cells in the drift chamber is required since the angular distribution of the decay products is rather isotropic. A spatial point resolution of 200 μm, with a high and well controlled efficiency is needed: the 12,582 cells are approximately square 3×3 cm^2 side (2×2 cm^2 for the inner 12 out of 48 layers), 3:1 field to sense ratio, and only alternating stereo wires (60 $\div$ 150 mrad) for a grand total of more than 52,000 wires;
- light materials were chosen to minimise multiple scattering, to have a good momentum resolution (in a 0.6 T magnetic field) at low momenta and to minimise conversions of low energy photons: carbon fiber composite for the mechanical structure, ultralight gas mixture, He 10%-iC_4H_{10} 90%, 80 μm Al 5056 (Ag plated) field, 25 μm W (Au plated) sense wires, for an overall thickness of the chamber, including front-end electronics, of $\simeq$ 0.1 X_0.

2 Chamber Construction

The two spherical (9.7 m curvature) carbon fiber end-plates, 8 mm thick, (with a 30 μm Cu foil glued on the external surface) are connected by 12 carbon fiber rods. Since the total load of the wires tension is $\simeq$ 3,500 kg, an external carbon fiber ring is used to recover the 3 mm deformation of each end-plate: the ring extert a radial force to the end-plates - through 48 screws monitored by means of strain gauges - which causes a longitudinal displacement in the direction opposite to that of the wires tension load. The procedure of deformation recovery has been successfully tested up to a static load of 5,000 kg. A

[†] *Contributed paper to the VII Pisa Meeting on Advanced Detectors, Elba Italy, May 25-31, 1997*

carbon fiber cylinder, 0.7 mm thick, provides the inner coverage and 12 carbon fiber panels will close the chamber.

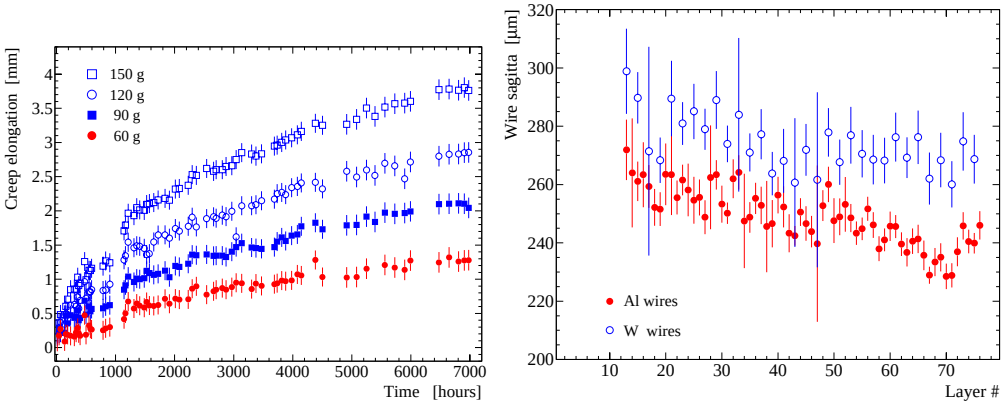

(a) (b)

Figure 5: The sagittae (b) of the aluminum wires are smaller immediately after stringing, since the elongation from creeping (a) is taken into account.

A number of tests have been performed on the wires: systematic measurements of wire linear density, Young modulus, as well as aging tests which show a negligible gain loss (5% after 30 years of KLOE operation [5]). A sample of aluminum wires has been subjected to constant load creep tests (total duration 10 months): a total elongation of about 1.5 mm is expected for the typical field wires tension, so that the field wires are strung slightly overtensioned (fig. 5).

3 Chamber Stringing

The stringing of the chamber is performed horizontally, in a clean room (class 1,000) by means of a semiautomatic system [6]:

- the two end-plates are supported and rotated by a special rig (accuracy at 2 m radius ~ 100 μm);
- a 3 axes robot brings the wire from one end-plate to the other (accuracy ~ 500 μm);
- two external stations tension the wire at the nominal mechanical tension and crimp the feed-throughs.

All axes are moved by step motors and are coupled to incremental encoders for position monitoring. The operations of wire feed to the robot and wire insertion into the feed-throughs are performed manually.

In order to get uniform sagittae the mechanical tension of the wires is measured by means of an electrostatic resonance method: the mechanical resonance of the wire is

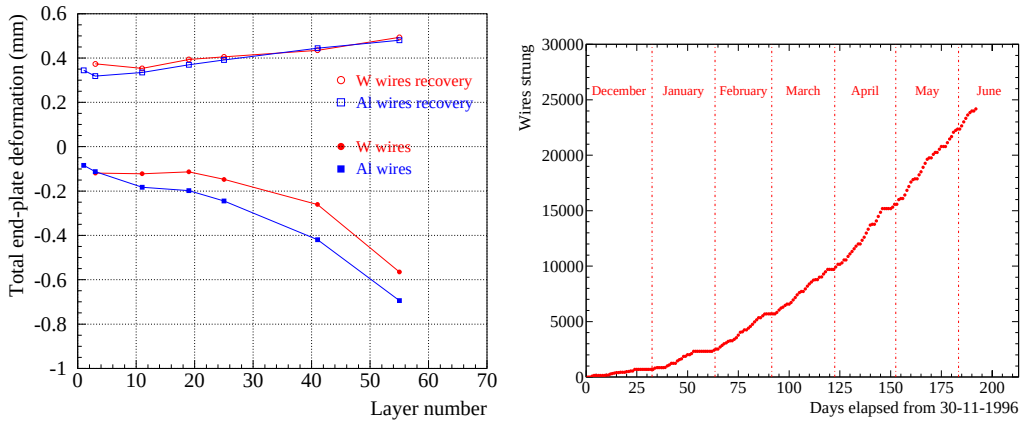

(a) (b)

Figure 6: (a) The deformation of the end-plates and its recovery are monitored by measuring the mechanical tension on a sample of wires; (b) The integrated "stringosity", defined as total number of wires strung as a function of the elapsed time of stringing.

detected by measuring the capacitance to the nearby wires [7]. Since this method does not require any magnetic field, it can be used to monitor any wire at any time. The sense wires are also tested at 3 kV voltage for leakage current measurements in order to identify short circuits or damaged wires. The external ring is tensioned every 300÷350 kg of wire load, in order to recover the wires tension loss due to end-plates deformation. The deformation is monitored on a sample of wires (on different layers) by measuring the wire tension loss, using the Young relation:

$$\frac{\Delta L}{L} = \frac{\Delta T}{EA}$$

where the Young modulus times the cross section area, EA, has been measured for a sample of wire spools and $\Delta L/L$ is the relative wire elongation. The deformation due to the load of wires strung in the period of 25 days is shown in fig. 6(a) together with the recovery: the difference in wire tension loss between aluminum and tungsten wires is due to the creep effect.

4 Conclusions

Stringing of the KLOE Drift Chamber began on 30 November 1996 and is now proceeding an average rate of 8,000 wires per month (fig. 6(b)), with a low percentage of replaced wires ($\sim$ 1.2%). A number of quality tests are performed on the wires and the end-plates deformation is monitored. The plate deformation due to the wire load is successfully recovered by means of the tensioning ring.

References

1. The KLOE Collaboration, *The KLOE Central Drift Chamber. Addendum to the KLOE Technical Proposal*, LNF-94/028(IR) (1994).
2. F. Lacava for the KLOE Drift Chamber Group, *Nucl. Phys.* **B54**, 327 (1997).
3. S. Spagnolo for the KLOE Drift Chamber Group, *these proceedings, poster session*.
4. G. Finocchiaro for the KLOE Drift Chamber Group, *these proceedings, Particle Identification session*.
5. G. Bencivenni *et al.*, *KLOE note* 143 (1995).
6. G. Bencivenni *et al.*, *KLOE note* 149 (1995).
7. V. Kulikov *et al.*, *these proceedings, poster session*.

Electrostatic Digital Method of Wire Tension Measurement for KLOE Drift Chamber [†]

Abstract

For the first time an electrostatic method of wire tension measurement (WTM) is used for drift chamber construction. It became possible due to digital approach to sense the wire oscillations induced by alternating potential. The method has excellent signal-to-noise ratio, high accuracy which is well above the stringing requirements and reasonable measuring time. WTM system implemented in CAMAC-Machintosh-Labview environment is now in use for stringing of KLOE drift chamber and for monitoring of the end-plate deformations.

WTM is always used during construction phase of wire chambers for stringing control. The only method of WTM which has been used up to now is the magnetic one which is based on a measurement of a resonance frequency of a wire oscillations induced by alternating current in magnetic field. For large drift chambers (DC) necessity to have a magnetic field about 199 Gs in large volume adds serious problem to already complicated and time consuming stringing procedure. For largest in a world DC of KLOE experiment with its 3 m length and 4 m diameter we decided to use another alternative - electrostatic method which is known from early days of MWPC but has been tried with very limited success because of very small signal. We have found a new solution to detect wire oscillations which has good sensitivity to construct reliable WTM system. An alternating high (1 kV) voltage is applied to a wire with respect to other wire(s) to excite forced mechanical oscillations. The periodic change of the wire capacitance to other wire(s) modulates a frequency of HF (10 MHz) LC-generator coupled to the wire. This frequency is measured in two successive quartz stabilised time intervals equalled to half-period of driving voltage. The difference between these frequencies is a measure of a wire oscillation amplitude. Driving voltage and gate pulses are computer synthesised. Changing the driving voltage in small steps an excitation curve of mechanical resonance of the wire is obtained and resonance frequency is extracted by fitting procedure. In Fig.1 a typical resonance curve for a wire in KLOE DC is shown for the case when capacitance between a wire and inner tube is measured. Even now when nearly half of the wires have been strung and the wire-tube distance is near 1 m we have no problems with WTM in this configuration.

[†] *Contributed paper to the VII Pisa Meeting on Advanced Detectors, Elba Italy, May 25-31, 1997*

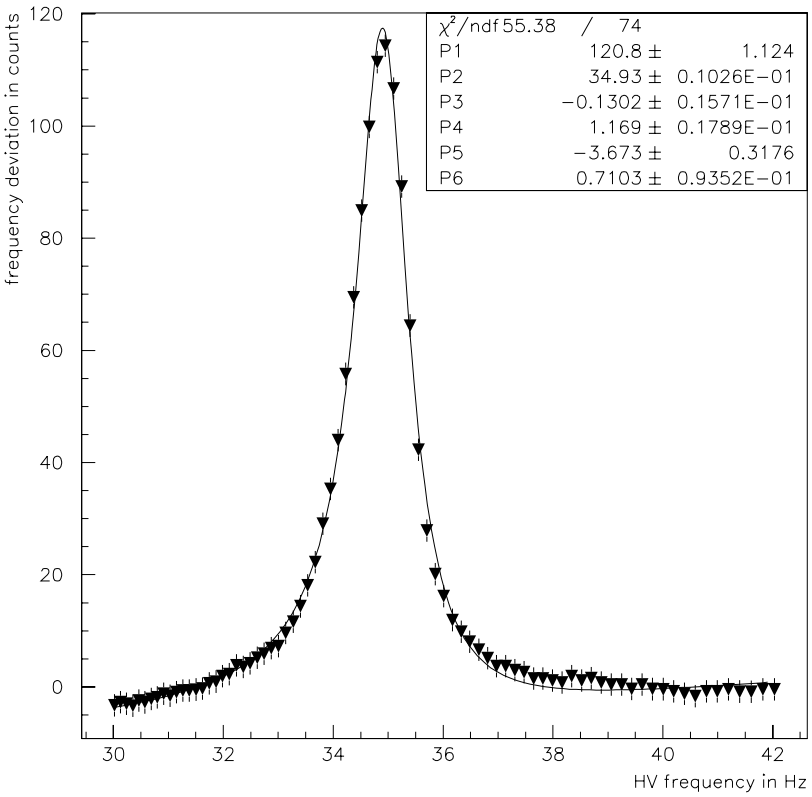

Figure 7: An example of mechanical resonance curve for a wire in KLOE DC.

Results from the Full Length Prototype of the KLOE Drift Chamber †

Abstract

A full size prototype of the KLOE drift chamber has been built and successfully exposed to a 50 GeV/c pion beam at CERN. The features of the cell response and the performances of the detector in terms of space and energy resolution are presented.

The Drift Chamber (DC) [1] of the KLOE experiment [2] is a rather unconventional detector due to the large size (2m radius and 3.2m length), to the choice of light materials (carbon fiber walls, 80μm $IHEP$ Al field wires, long X_0 gas mixture 90%He10%iC_4H_{10}) and to the all stereo geometry. In order to check the design performances a full size prototype was built [3] which consists of 30 coaxial layers, with radii between 28cm and 104cm, of squared single sense wire cells, $3\times\pi$ cm^2 in size ($1.5\times\pi/2$ cm^2 in the ten innermost layers), strung at alternating sign stereo angles in the range of 50÷120mrad between conical, 6.2mm thick, end plates made of carbon fiber. The detector was operated at a gain of 10^5, provided by 1950V on the 25μm $IHEP$ W anode wire. A very stable and noise free operation was observed for thresholds as low as 2mV (1/8 of the one electron equivalent with the 1mV/fC gain of the KLOE DC preamplifier, Tektronics VTX). A set of 27×10^6 tracks from 50GeV/c pions, collected at the SPS T1-X7 area, allows to study the cell response as a function of the relevant parameters: ϕ the angle between the track and the radial direction, β_u and β_l describing the cell shape deformations due to the cell arrangement on circular layers and to the stereo configuration (see fig.8). The prototype has been used as self tracking device and a special algorithm, described in detail elsewhere [4], for straight track reconstruction in the all stereo geometry (for which the pattern recognition task is highly non trivial) was applied to the analysis of the data sample.

The correlation, $r(t_d)$, between the distance of closest approach (DCA) of the track to the hit sense wire and the drift time, t_d, is parametrized by three 4th order polynomials connected at $t_d = 450$ns (i.e. 1/2 of the maximum impact parameter for $\phi = 0^0$), where $r(t_d)$ is continuous and differentiable, and at $t_d = 880$ns (~ 1.4cm), where only the function continuity is preserved‡. While the first branch polynomial is stable as ϕ, β_l and β_u change, the anysotropy and the cell deformations affect $r(t_d)$ at impact parameters larger than 1cm by amounts much larger than the resolution. Since $|\beta_l| < 9^0$, two sets of curves ($\beta_l > 0$ and $\beta_l < 0$) in each ϕ slice are enough to describe the cell behaviour in the lower half; in the cell upper half, β_u ranges between $\pm 30^0$ and, hence, the parameterization of $r(t_d)$ is split in a number of β_u slices, increasing with $|\phi|$ from 1 up to 7, within each ϕ slice. By exploiting the cell symmetries ($r(t_d; \phi, \beta) = r(t_d; -\phi, -\beta)$

† *Contributed paper to the VII Pisa Meeting on Advanced Detectors, Elba Italy, May 25-31, 1997*

‡ Here, as well as in the following, we refer, without loss of generality, to the $3 \times \pi$cm^2 cells, where a slightly lower average drift velocity, 1.6cm/μs compared to 2.1cm/μs in the smaller cells, enhances the edge and anisotropy effects.

and $r(t_d;45^0-\phi,\beta_l)=r(t_d;45^0+\phi,\beta_l)$ for $\beta_l \to 0$), a total number of 36 parameterizations of $r(t_d)$, coupled to the corresponding resolution function $\sigma(t_d)$, has been proven to provide a complete prediction of the cell response (as an example, a set of such curves is shown in fig.8). The trends of both $r(t_d)$ and $\sigma(t_d)$ observed from the data are nicely confirmed by Monte Carlo simulations based on the GARFIELD package.

The space resolution, of the order of 120μm for impact parameters between 0.2 and 1.0cm (well below the KLOE target of 200μm which will be multiple scattering dominated), can be decomposed into several contributions: primary ionization statistics, longitudinal diffusion, electronic noise and extrapolation error. The analysis allows to get a measurement of the mean free path for ionization in $90\%\mathrm{He}10\%i\mathrm{C}_4\mathrm{H}_{10}$ $\lambda=(597\pm43)\mu$m (in agreement with [5]) and of the ratio between diffusion and drift velocity $2D(E)/v_d(E)=(3.4\pm0.4)\cdot10^{-4}$ cm (see ref. [6]). The extrapolation error accounts for $(30\pm3)\mu$m and the overall time resolution (digitizing time and trigger jitter) comes out to be (3.6 ± 0.3)ns. As a result of the space resolution, angular resolutions of the order of 0.2mrad in the transverse plane and of 2mrad in the longitudinal plane have been evaluated from the width of the director cosine distributions of radial tracks crossing all the 30 layers (the beam divergency has been safely neglected). The hardware efficiency of the cell, averaged over the cell area, exceeded 99.7% when a discrimination threshold of 4mV, corresponding to a noise frequency per event of 0.002 hits/cell, was set in. Almost 50% of the inefficiencies, clusterized within 1mm from the cell edge, are due to the cut of the drift times longer than 2μs. The average probability of getting a measurement of the drift distance in agreement with the extrapolated DCA within 1σ is $(66.03\pm0.04)\%$, for $\phi=0^0$, which entails a degree of knowledge of $r(t_d)$ and $\sigma(t_d)$ better than 97.75%.

Finally, charge measurements confirme claims of good dE/dx performances of the gas mixture [7]. A 27% resolution is observed on single cell measurements, while a 15% truncated mean, over the average number of hits for tracks in the $K\to\pi^+\pi^-$ process, allows to pull down the energy resolution to 3.5%.

In conclusion, the full size prototype of the KLOE DC, besides showing that the challenging conceptual design of the detector will successfully fulfill the requirements of resolution in reliable operation conditions, has provided also a useful first level calibration of the cell response.

References

1. The KLOE Collaboration, LNF-93/002(IR); M. Primavera, NIM**A379**(1996)414
2. The KLOE Collaboration, LNF-92/019(IR)
3. F. Grancagnolo, NIM**A367**(1995)108; S. Spagnolo, Nucl.Phys.B**54B**(1997)70
4. M. Primavera and S. Spagnolo, KLOE note 153, Dec. 1995; G. Cataldi *et al*, "Straight track reconstruction in all stereo drift chambers", to appear in NIM
5. G. Cataldi *et al*, NIM**A386**(1997)458; A. Sharma and F. Sauli, NIM**A350**(1994)470

6. V. Palladino and B. Sadoulet, NIM**128** (1975) 323; V. Golovatyuk *et al*, "Single electron longitudinal diffusion in helium-isobutane gas mixtures", to appear in NIM

7. G. Finocchiaro *et al*, these Proceedings

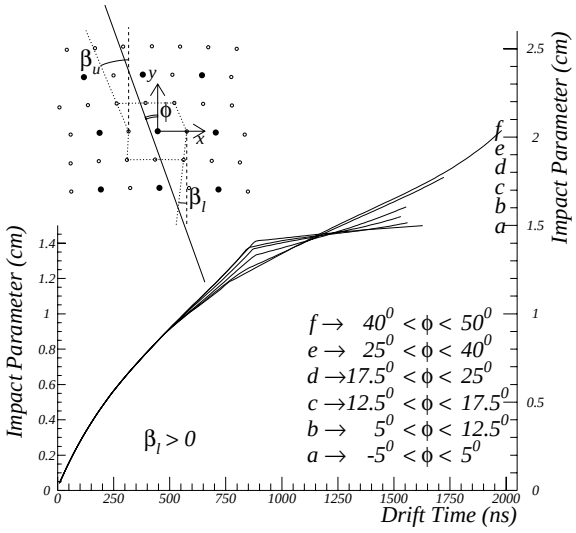

Figure 8: Time to distance relations, $r(t_d)$, for the lower half of cells with $\beta_l > 0$ crossed by the track at angles ϕ within the intervals specified for each curve. The layout of the cell cross section shows the definition of the angles affecting the cell response.

dE/dx measurement in a He-based gas mixture †

Abstract

The performance of a prototype drift chamber operating in a He-based gas mixture as a specific ionisation detector is presented. In spite of the small number of primary ions, Helium performs quite satifactorily in measuring energy losses for charged particles: with $50\,\mathrm{GeV}/c$ pions, we have measured in a $90\%\mathrm{He}-10\%i\mathrm{C}_4\mathrm{H}_{10}$ mixture a relative energy loss resolution of 3.1% with 75 samples $3\mathrm{cm}$ long, using a modified Truncated Mean technique with 80% accepted fraction.

The dependence of the resolution on several parameters such as the operating voltage, the truncation fraction, the number and length of the samples is discussed.

1 Introduction

As a result of the R&D programme for its big drift chamber [1)], the KLOE collaboration chose $90\%\mathrm{He}-10\%i\mathrm{C}_4\mathrm{H}_{10}$ as the optimal gas mixture for its long X_0 ($\simeq$1300m), excellent operational stability, high efficiency, good spatial resolution and, last but not least, non flammability and simplicity (it is a binary mixture). In this paper we present results demonstrating that its performances are extremely good also from the point of view of the $\mathrm{d}E/\mathrm{d}x$ measurement.

† *Contributed paper to the VII Pisa Meeting on Advanced Detectors, Elba Italy, May 25-31, 1997*

2 Experimental setup

The analysis described in this paper is relative to data collected on a $50\,\mathrm{GeV}/c$ pion beam at the CERN SPS in september '94 with a small size prototype of the KLOE drift chamber (prototype 0.3). A detailed description of the prototype and of the data taking conditions can be found in [2]; only the points relevant to the $\mathrm{d}E/\mathrm{d}x$ measurement are mentioned in the following. The prototype consists of an array of 7×7 approximately square cells of $(3\times\pi)\mathrm{cm}^2$ area each, with a field to sense wire ratio of 3:1. We consider in the present analysis only the 25 innermost cells, whose gain is made homogeneous by the external ones, which act as guard wires. After preamplifiers with a gain of $1\,\mathrm{mV/fC}$ on a $50\,\Omega$ load [3] and post-amplifiers with gain $\simeq3$, the analog outputs from the sense wires were fed to LRS2249W ADC's with a $3.9\,\mu\mathrm{s}$ wide gate.

2.1 Data sample and quality cuts

We collected data at five HV settings, every 50V between 1750 and 1950V, both with and without a magnetic field of 0.6T parallel to the wires. At the two highest operating voltages there was a non negligible saturation of the ADC, hence the corresponding data have been used in the gas gain saturation studies, see next section, but not in the $\mathrm{d}E/\mathrm{d}x$ anlaysis.

The ADC spectrum in one of our 3 cm cells is shown in fig.9. A cell is defined as 'hit' if its ADC reading, pedestal subtracted, exceeeds three times the pedestal width. The relative width σ_{REL} of the peak is typically $\simeq25\%$. On average about 5 cells are hit [4]. We select a clean sample of events by further requiring to have at least 4 hit cells, a drift time of the first electron less than $2.5\,\mu\mathrm{s}$ and impact parameter less than 1.5 cm. The combined efficiency of these cuts is about 80%.

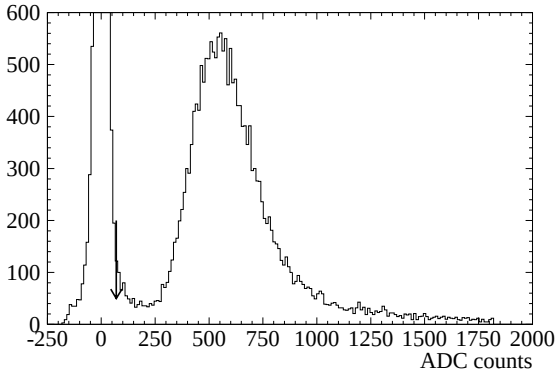

Figure 9: *Typical ADC spectrum. The arrow shows the three sigma cut.*

3 Results

After equalisation of the response of the cells,[‡] we calculate the Truncated Mean (TM) to estimate the most probable value of the energy loss distribution ($\mathcal{E}_{\mathrm{MP}}$). Truncated Means are plotted in fig.10 for different fractions of accepted events. We observe that in our $90\%\mathrm{He}-10\%i\mathrm{C}_4\mathrm{H}_{10}$ gas mixture the most probable energy loss ($\simeq136\,\mathrm{pC}$ at 1850V) is correctly reproduced accepting 80% of the hits. Since for a $50\,\mathrm{GeV}/c$ beam the energy loss, regardless of the particle species and the momentum bite of the beam itself, lays on the relativistic plateau, we can combine several 5-hits events to simulate arbitrarily long

[‡]We scale each ADC reading by the factor $\mathrm{MP_i}/\langle\mathrm{MP}\rangle$, $\mathrm{MP_i}$ being the Most Probable energy loss in the i-th cell, and $\langle\mathrm{MP}\rangle$ the same quantity averaged over all the cells.

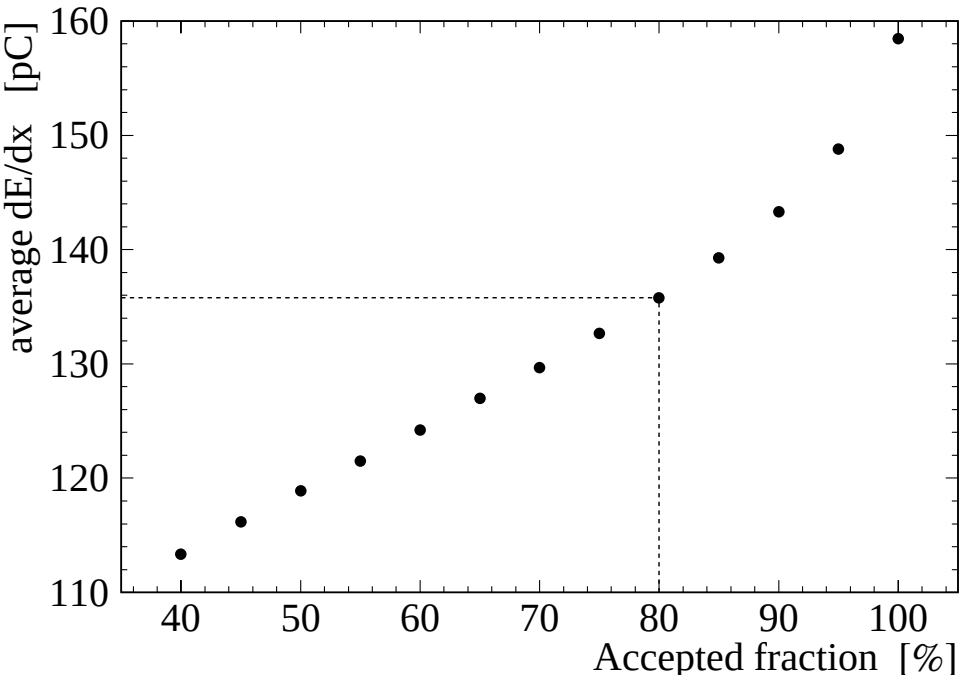

Figure 10: Truncated Means vs. accepted fraction.

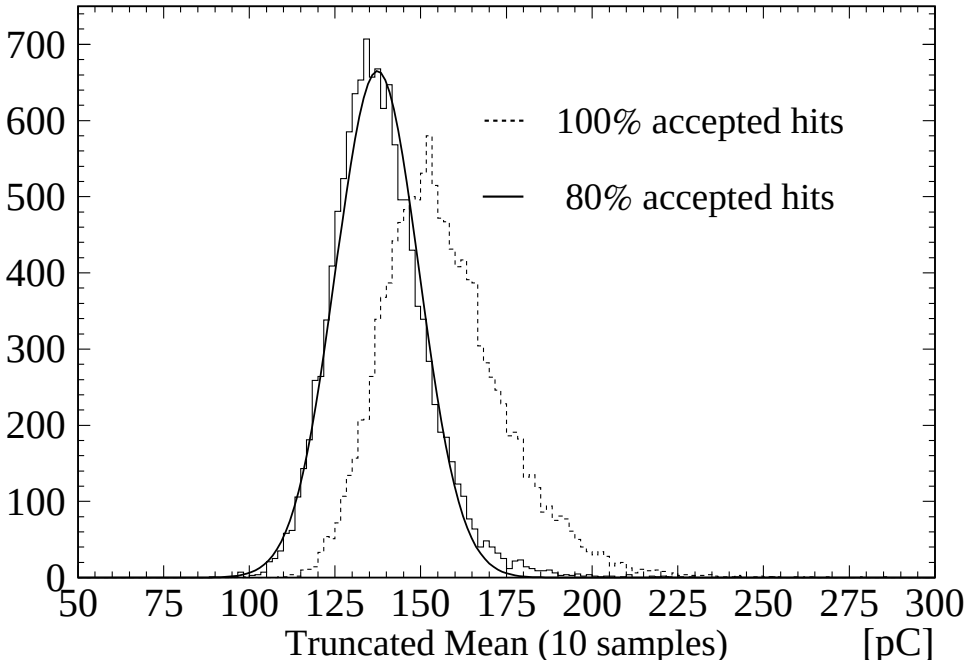

Figure 11: Effect of the Truncation in samples of 10 hits.

tracks. The effect of the truncation is pictorially shown in fig.11: even with samples of only 10 hits, the distribution of the average shifts towards the correct $\mathcal{E}_{\rm MP}$, shrinks considerably and becomes fairly gaussian at 80% truncation. Completely gaussian distributions are obtained for $\mathcal{N}$ (total number of hit cells) greater or equal to 20.

3.1 $\mathrm{d}E/\mathrm{d}x$ resolution

In fig.12 the $\mathrm{d}E/\mathrm{d}x$ resolution $\sigma_{\mathrm{d}E/\mathrm{d}x} \equiv \sigma(\mathrm{TM})/\langle\mathrm{TM}\rangle$ is plotted vs. the number of used hits (80% accepted fraction). A fit with a power function is superimposed to the points, showing that the scaling law is very close to the Poisson limit of -0.5. The resolution exhibits a mild dependence on the accepted fraction (fig.13): a broad minimum is observed between $\sim$60% and 90%, while both for bigger (inclusion of the Landau tail) and smaller accepted fractions (loss in statistics) $\sigma_{\mathrm{d}E/\mathrm{d}x}$ deteriorates.

3.2 Linearity of the measurement

Apart from trivial saturation of the ADC, pulse height saturation may originate from non linearity of the gas amplification. The latter may also result in an artificial reduction of the Landau tails, since at very big gains space charge at the anode could decrease the effective amplification.

Fig.14 shows the MP pulse height as a function of the operating voltage. Since we find the same slopes within the errors in the 'low' and the 'high' HV regimes, we conclude that there is no gas gain saturation. Saturation could also show up by a decrease of the collected charge with the drift distance: the ionisation clusters arrive more grouped in time to the anode if they originate from distant tracks, therefore saturation phenomena would be more likely. Fig.15 depicts the average collected charge vs. drift distance: we observe a 2% decrease of the collected charge over the entire cell width. This modest effect is however an upper limit to space charge effects, since the same trend could also be caused by the presence of electronegative agents in the gas mixture or by the finite integration gate.[§]

We measure essentially the same resolution at 1800 and 1850V, while at $1750\mathrm{V}$ $\sigma_{\mathrm{d}E/\mathrm{d}x}$ is $\sim$13% worse. Using 75 hits, which is an expected average over several reactions in KLOE, we measure therefore, with $50\mathrm{GeV}/c$ pions and 80% accepted fraction, a $\mathrm{d}E/\mathrm{d}x$ resolution of (3.3$\pm$0.1)%. The error is not only statistical, but includes variations of the cuts and run-to-run differences.

A magnetic field of 0.6T does not significantly affect this result, both because of the wide integration gate and of the small Lorentz angle in the mixture [2)].

[§]The wide gate of 3.9μs guarantees in our case that practically all the charge is collected by the anode.

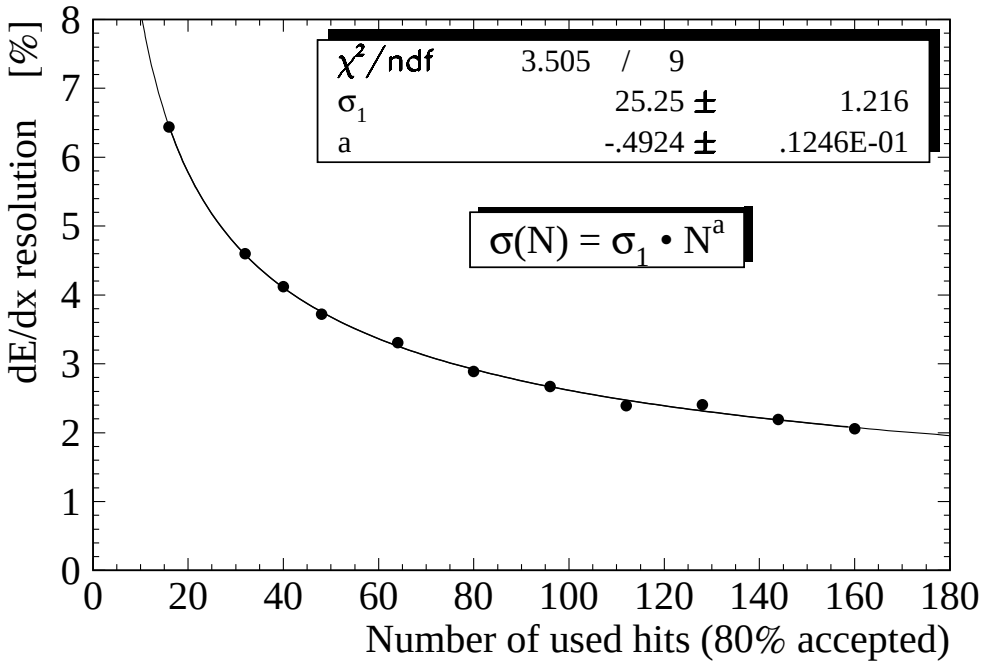

Figure 12: $\mathrm{d}E/\mathrm{d}x$ resolution vs. number of used hits.

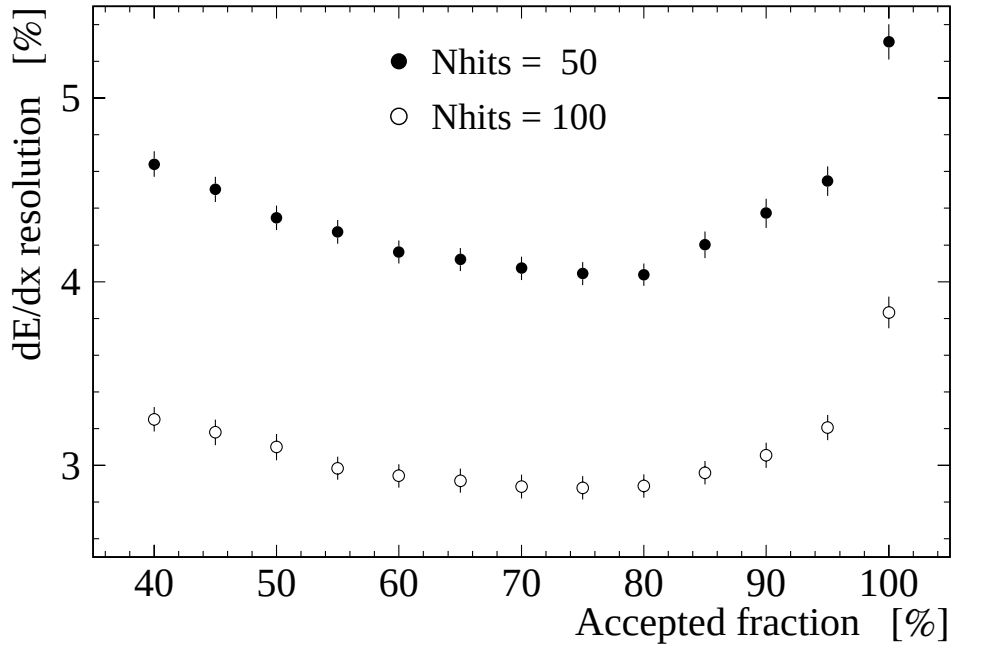

Figure 13: $\mathrm{d}E/\mathrm{d}x$ resolution vs. TM accepted fraction.

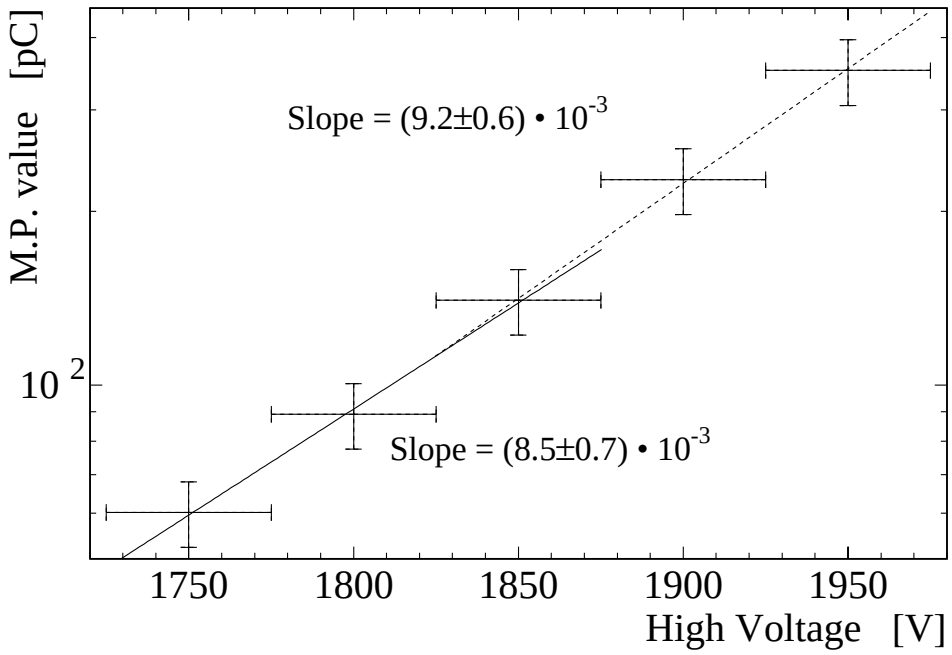

Figure 14: Most probable energy loss vs. operating voltage.

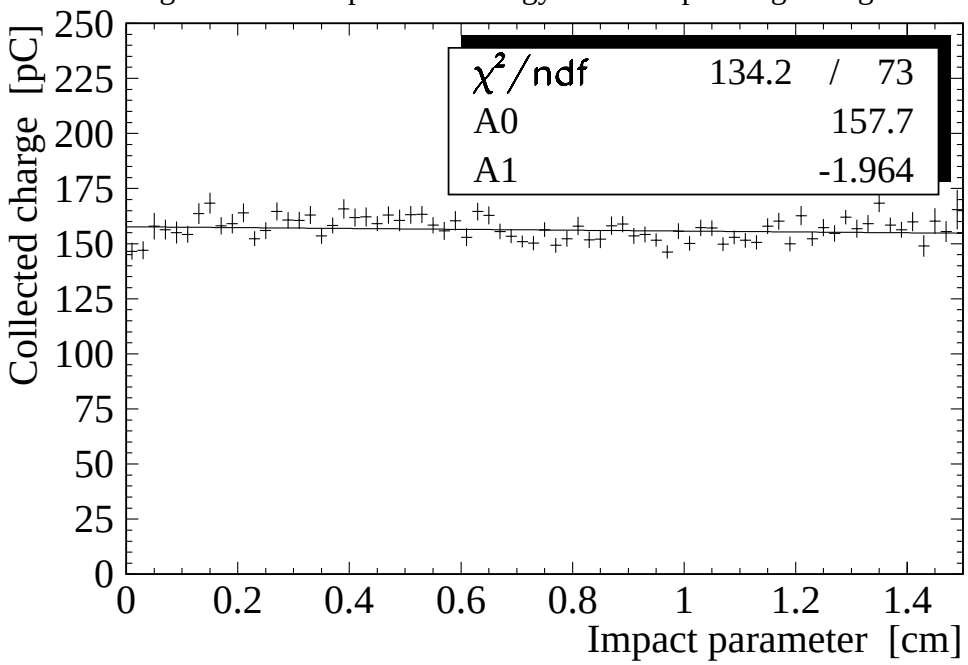

Figure 15: Collected charge as a function of the track's impact parameter.

3.3 Optimisation of the truncation fraction

To improve the analysing power of the $\mathrm{d}E/\mathrm{d}x$ measurement, we tune the accepted fraction of the TM on the shape of the particular sample under consideration. Using the correlation between accepted fraction a sample RMS we obtain a $\mathrm{d}E/\mathrm{d}x$ resolution of (3.1±0.1)%.

3.4 Resolution vs. sample thickness

The dependence of the $\mathrm{d}E/\mathrm{d}x$ resolution on the number $\mathcal{N}$ and the length x of the samples has been parametrised [5)] as $\sigma_{\mathrm{d}E/\mathrm{d}x} \propto \mathcal{N}^a \cdot x^b$; in the same reference the authors find for Argon $a = -0.46$, $b = -0.32$. In our mixture (fig.12), $a = -0.49 \pm 0.01$. To measure b, we have simulated 'supercells' of increasing length. From a fit to the ratio $\sigma_{\mathrm{REL}} \equiv \sigma_{\mathrm{peak}/\langle\mathrm{peak}\rangle \propto \mathrm{x}^{\mathrm{b}}}$ as a function of the size of the supercell, we obtain the value $b = -0.40 \pm 0.01$. Finally, we determine the difference $a - b$ by sampling a track with a given total length with supercells of different length; fitting the TM resolution of the supercells again with a power law, we find $a - b = 0.07 \pm 0.01$, consistent with the separate determinations of a and b.

We want to stress that this result stems from the small value of the cluster multiplicity and of the limited Landau tails in Helium: the difference between the a and b exponents is to some extent a measurement of skewness of the energy loss distribution: in a completely symmetric distribution the two effects of decreasing the number of samples and increasing the sample thickness would balance out.

4 Conclusions

The $\mathrm{d}E/\mathrm{d}x$ resolution in the gas mixture $90\%\mathrm{He}-10\%i\mathrm{C_4H_{10}}$ has been measured. Up to operating voltages of 1900V (gain of few 10^5 [2)]) we have found negligible saturation. The dependence of the resolution on the number and the length of the samples has been extracted. We expect, from these measurements, a specific ionisation resolution in the KLOE detector of about 3.5%.

References

1. P. Valente for the KLOE Drift Chamber Group, *these proceedings*, and references therein.

2. F. Lacava for the KLOE Drift Chamber Group, *Nucl. Phys.* **B54**, 327 (1997).

3. M.Carletti, G.Felici, P.Locchi, KLOE internal note #66, Oct. 1993, unpublished.

4. For a detailed discussion of these and other points in this paper see G. Finocchiaro, M. Piccolo and P. Valente: $\mathrm{d}E/\mathrm{d}x$ resolution in a $90\%\mathrm{He}-10\%i\mathrm{C_4H_{10}}$ gas mixture with $50\,\mathrm{GeV}/c$ pions, KLOE internal memo # 33, Oct. 1995, unpublished.

5. W.W.M. Allison and J.H. Cobb, *Ann. Rev. Nucl. Part. Sci.* ***30****, 323, (1980).*

Performances of a Multichannel 1 GHz TDC ASIC for the KLOE Tracking Chamber †

Abstract

The KLOE TDC is a multichannel common start/stop time-to-digital converter, with 32 channels per chip. The time measurement is done digitally by counting $1\ GHz$ clock periods generated by an internal Delay Locked Loop DLL. The circuit has a $500\ ps$ resolution over a programmable time window of up to $65\ \mu s$, and is capable of recording up to 16 rising or falling edges per channel. It has a double edge resolution of $5\ ns$ and is capable of resolving a pulse of $3\ ns$ width.

The experiment requires that the data read-out does not introduce dead time on top of the $2\ \mu s$ digitization time of the calorimeter electronics. A multi-event architecture has been implemented to satisfy this requirement. The experimental DAQ chain can read framed and zero suppressed data from the internal buffers at a maximum data throughput of $720\ Mbit/s$ while the ASIC is recording new events.

The chip has been realized as a full custom device in $0.5\ \mu m$ CMOS technology, it has been fully tested both in the laboratory and on a test beam, all the specifications are met.

A total of 15000 channels are being produced for the KLOE experiment.

1 Introduction

The KLOE wire chamber [1)] is a cylindrical $4\ m$ diameter, $3.2\ m$ long tracking chamber. A $90\%(He) - 10\%(iC_4H_{10})$ gas mixture and an approximately square $3 \times 3\ cm^2$ cell geometry, preserve the chamber transparency ($X_0 = 1300\ m$) to low energy charged particles, down to $50\ MeV/c$. The maximum drift time is $\sim 2\mu s$ and the required spatial resolution of $\leq 200\ \mu m$. The contribution of the digitization electronics to the spatial resolution is negligible when the TDC resolution is $\sim 1\ ns$.

The chamber volume is currently being equipped with 12600 sense and 53000 field wires.

The number of channels to be equipped and some other requirements which will be shown later have prompted the necessity to design an ASIC dedicated to the chamber time measurement. The high integration of the circuit made it possible to design a 96 channels TDC on a 6U VME board.

The KLOE experiment [2)] is capable of giving the first level trigger ($T2$) [3), 4)] with a variable latency smaller than $3.0\mu s$. The $T2$ signal will be used as a common stop for the TDC. The TDC measures the time differences between pulse edges of the front end discriminator and $T2$. The time window for accepted hits is programmable between $64\ ns$ and $65\ \mu s$ (see Fig.16). The circuit is capable of recording up to 16 edges per channel,

† *Contributed paper to the VII Pisa Meeting on Advanced Detectors, Elba Italy, May 25-31, 1997*

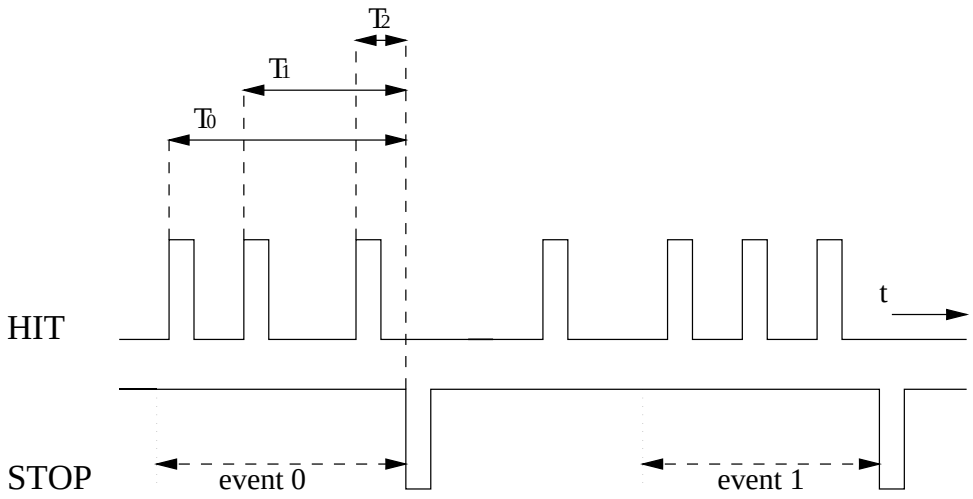

Figure 16: Common stop operation

rising or falling; noisy channels can be masked.

The circuit has been designed to be operated also in common start mode (see Fig.17). In this case the circuit measures the time differences between the signal edges and the first edge of the start. It is possible to record a new event $35\ ns$ after the arrival of each stop/start (STOP) signal.

2 Circuit description

A full description of the circuit has been already given elsewhere, [5], [6], [7]. The overall scheme of the circuit is shown in Fig.18.

The reference time is given by an external $160\ MHz$ quartz. This frequency is multiplied internally to $960\ MHz$ by a DLL.

The available CMOS technology has low gate delays and it is possible to generate internal high frequency clocks and counters and build a time measuring device simply by counting the number of clock periods between two signal edges. Since the chosen process technology has a typical gate delay of $\sim 100\ ps$, short compared to the required clock period, a digital control of the DLL has been realized.

The DLL consists of a cascade of 6 identical noninverting delay stages (see Fig.19). Each stage has a phase difference of $T_{in}/6$, where $T_{in} = 1/160\ MHz$, respect to the input clock.

Each stage consists of 16 inverters and a multiplexer. The DLL phase detector drives a sequencer which adds or removes a number of inverter pairs in the delay chain, always equalizing the total delay of each stage with respect to each other. The output of each of the 6 delays is fed to a combinatorial circuit which generates the required $960\ MHz$

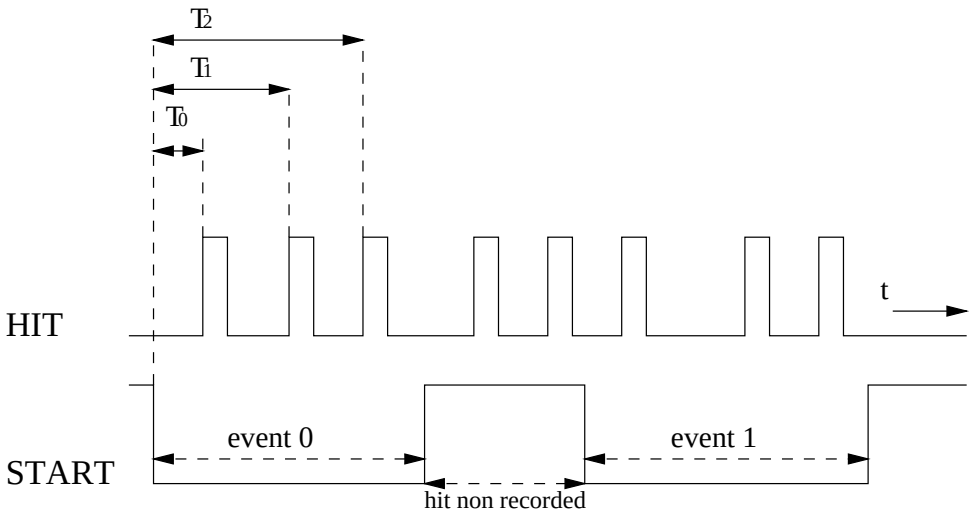

Figure 17: Common start operation

clock. A programmable width Gray counter, up to 16 bit wide, is driven directly by this clock.

When a new signal edge is presented at one of the channel inputs, the hit control logic writes the current value of the free running counter in a 16 hit deep FIFO. The hit control logic contains also the masking logic and has been designed for a double edge resolution of $8\ ns$. Each channel contains also a hit removal circuit to discard old hits, i.e. hits fallen out of the programmable time window. The FIFO empty flag ouputs are used as a prompt trigger to warn of the presence of new hits in the chip.

Four FIFOs are available per channel, to be able to readout old triggers while recording new ones. Also four $STOP$ registers are necessary; they contain the value of the Gray counter on the arrival time of the $STOP$ edge. In order to minimize the buffer occupancy, the buffer control logic switches to a new buffer only if at least one hit is present in one of the 32 FIFOs.

A 24 bit asynchronous parallel bus, running at a maximum frequency of $30\ MHz$, is used both for readout and initialization of the chip. The events are readout one after the other (Sequential Readout Mode) with the hits sorted by channel number. The exact number of events in the chip is continuously available off chip via dedicated lines.

The data readout can follow also a Readout upon Event Request protocol, as required by the KLOE readout architecture.

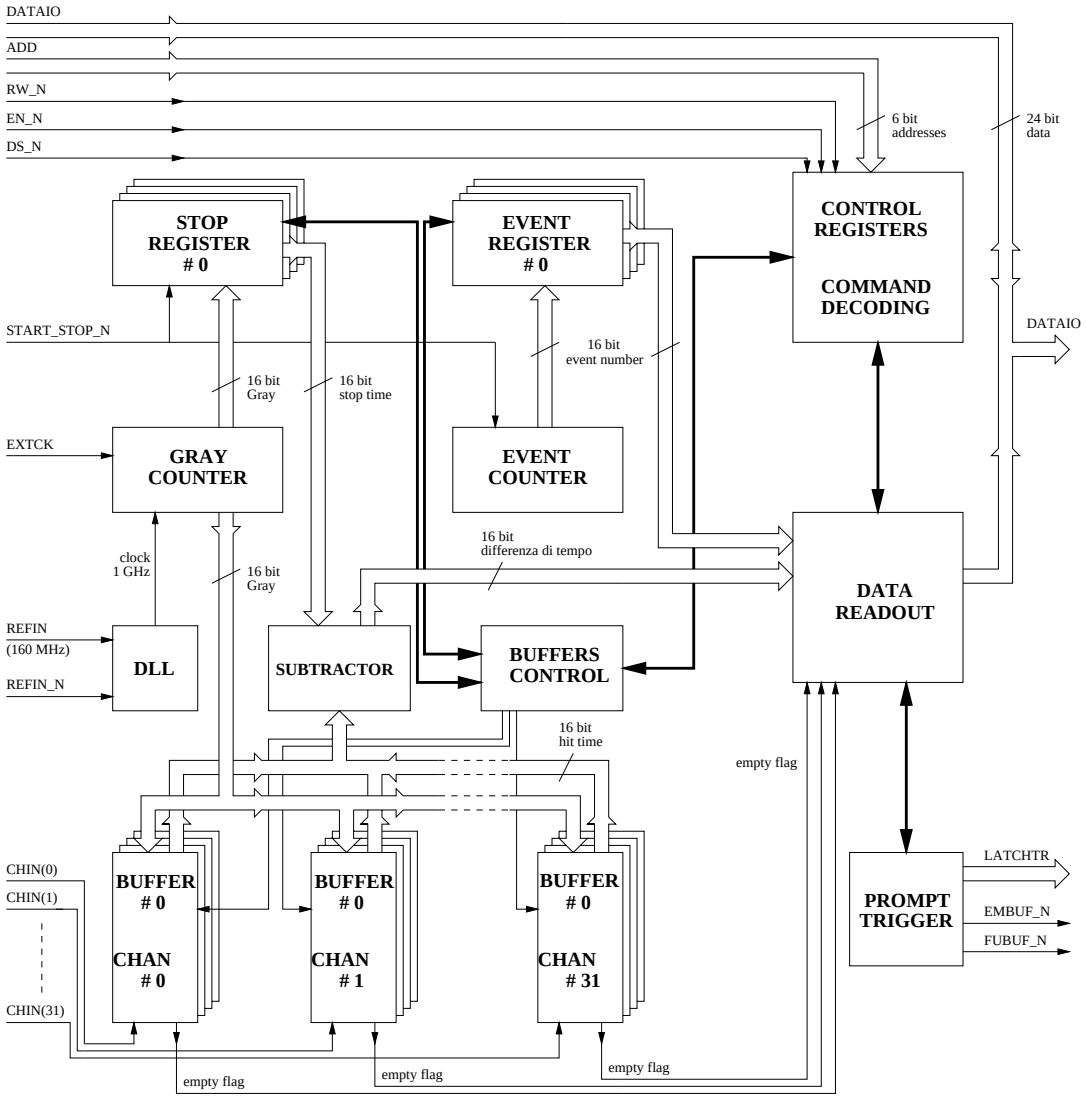

Figure 18: KLOE TDC block diagram

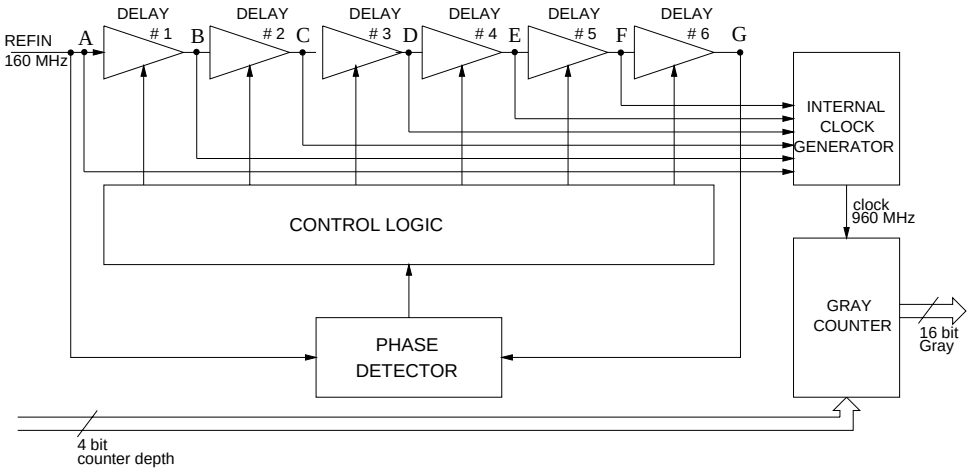

Figure 19: Scheme of DLL

3 Chip design

A detailed model has been used at the beginning as the design specification and to partition the chip in functional blocks. Input-output (IO) signals of each block have been defined at this level. This first model has been fundamental to evaluate the gate count and cost; most of the non-critical control parts have been synthesized directly from this model. Each block has been substituted as soon as available with the gate level model and simulated in conjunction with the rest of the design, to check whether the implementation was correct. In parallel with this design flow, a simpler behavioural TDC model has been written, to generate the test vectors, and check the gate level model. The layout of the chip and gate level design of the full custom blocks have been realized by the Bull microelctronics design center of Les Clayes Sous Bois, France.

The 32 channels are organized in four quadrants of 8 channels each. Along the main axes runs the 16 bit Gray counter bus. Each channel has been implemented as a full custom block from a $VHDL$ [8] structural description ($2.5 \times 0.3\ mm^2$ area). The DLL and Gray counter is on the right hand side, close to the channel memories. The rest of the logic, the control parts, the time subtractor, the $STOP$ and Event registers, the event request logic, the event counter are on the top. They have been synthesized from VHDL constructs.

The chip has been built in a $0.5\ \mu m\ CMOS\ \ 3.3\ V\ \ HCMOS5S$ process by SGS-Thomson. The total area of the chip is $\simeq 10 \times 10 mm^2$, with about $5 \cdot 6.4 \cdot 10^5$ transistors. The chip is packaged in a 160 pin ceramic PGA (Pin Grid Array). All the IO buffers are designed to be TTL compatible; the reference clock input is PECL differential for better noise rejection. The total power dissipation is $\simeq 1\ W$ when in operation. It can be put in standby by switching off the DLL circuit, in this case the power consumption goes down

to $180\ mW$. No heat sink is needed.

4 Performances

The first 8 inch prototype wafer has been produced in May 95. 80 good dies passed the test vectors, out of 268 ($\simeq 0.3$ yield). The second and final foundry run in March 96 fixed also a design fault of the channel input protection.

The full production of 600 packaged chips has been delivered at the time of writing. A 32 channels VME board [9)] has been designed to characterise the chip. The first tests have focused on the performances of the DLL circuit, which was found fully functional. A deviation from the delay uniformity of $\sim 200\ ps$ has been measured directly from the clock test output pin (Fig.20), it is comparable to the minimum delay step which can be inserted or removed in the chain by the DLL control unit.

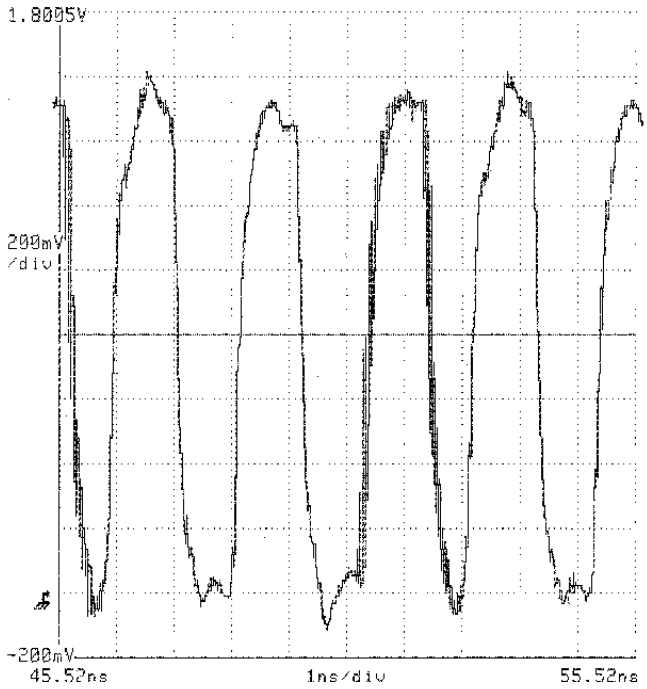

Figure 20: DLL monitor output (480 MHz)

The upper limit on the differential non-linearity of each range has been measured looking at the circuit response to a flat input time difference spectrum, generated using two out of phase pulse generators (one hit and one common stop generators), running at different frequencies. An upper limit of $0.12\ LSB$ has been found taking $\simeq 4.2 \cdot 10^6$ events, giving an average of 64 hits per channel, on the full 65536 channels counting range (Fig.21).

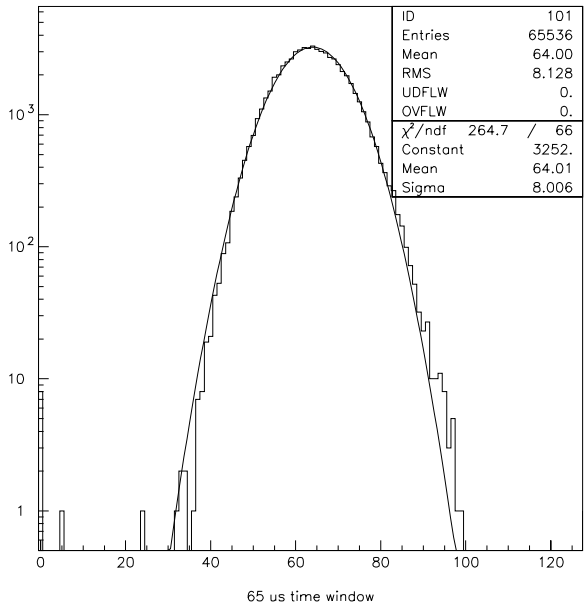

Figure 21: The total counts per channel distribution, shown for the $65\ \mu s$ range, has been generated with $\simeq 4.2 \cdot 10^6$ events. A gaussian fit is superimposed.

Integral non-linearity has been measured with a TEK HFS9200 pulse generator (RMS jitter of the time base equal to $15\ ps \pm 0.05\%$ of the delay). An upper limit of $0.2\ LSB$ has been measured in the $2\ \mu s$ range, the measurement being dominated by the generator time base jitter.

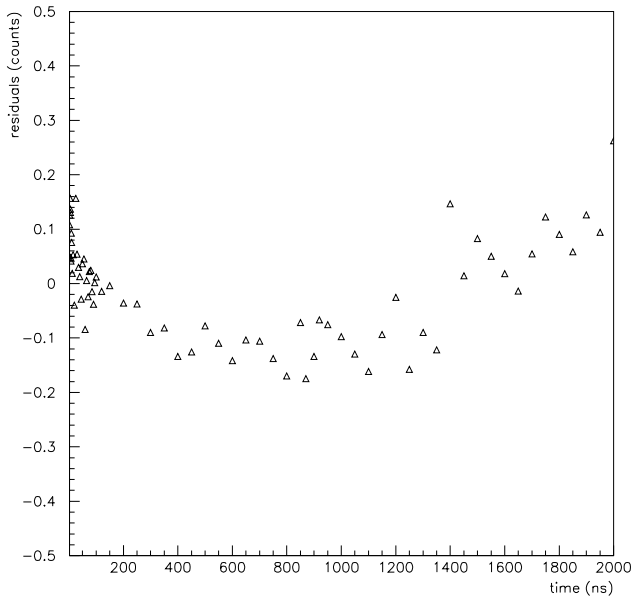

Figure 22: Integral non linearity in the $2\ \mu s$ range

The time resolution of the TDC has been measured with the same setup. In Fig.23 the resolution in the range $0 - 20\ \mu s$ is shown. It is compatible with the expected value of $1\ ns/\sqrt{6}$ (the time difference is obtained with two measurements). The performances of the circuit to the double edge resolution have been found better than the specifications. In Fig.24 a $5\ ns$ pulse at $1\ \mu s$ from the ST signal is recorded. No hit loss has been found during the measurement time.

5 Conclusions

A TDC circuit for the tracking chamber of the KLOE experiment has been developed. The 32 channel chip fully satisfies the design specifications and its performances make it available for other applications.

A 96 channels VME board is being built at the time of writing, 130 of which will equip the KLOE chamber readout system next year.

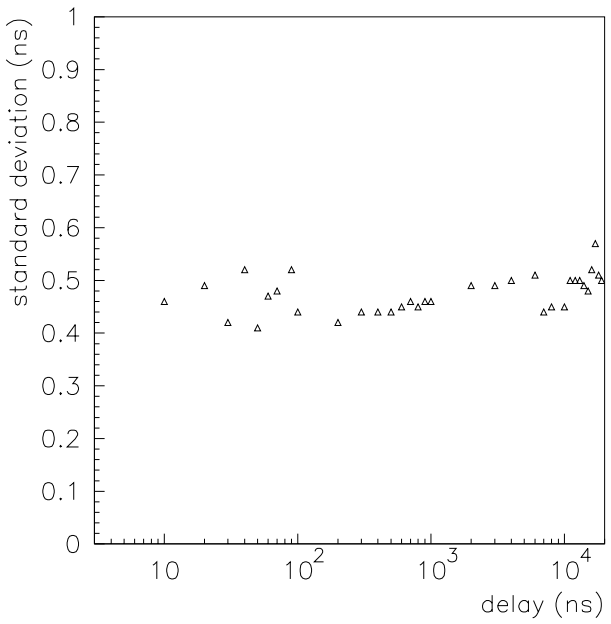

Figure 23: Time resolution in the $20\mu s$ range.

References

1. The KLOE central drift chamber: addendum to the KLOE technichal proposal. By KLOE Collaboration (A. Aloisio et al.). LNF-94-028-IR, Jun 1994.

2. KLOE collaboration, the KLOE detector, Technichal proposal, LNF-94/028, 1994.

3. The KLOE trigger system. (addendum to the KLOE technichal proposal). By KLOE Collaboration (A. Aloisio et al.). LNF-96-043-IR, Sep 1996.

4. The KLOE data acquisition system: addendum to the KLOE technichal proposal. By KLOE Collaboration (A. Aloisio et al.). LNF-95-014-IR, Mar 1995.

5. M. Passaseo, E. Petrolo, S. Veneziano; A Multichannel TDC Integrated circuit for Drift Chamber Readout - TDC chip specifications. KLOE MEMO 104/97.

6. M. Passaseo, E. Petrolo, S. Veneziano; A TDC integrated circuit for drift chamber readout. Proceedings of 1994 Vienna Wire Chamber Conference, Nuclear Instruments Methods Phys. Res. A 367 (1995) 418-421.

7. M. Passaseo, E. Petrolo, S. Veneziano; Design of a multichannel TDC integrated circuit for drift chamber readout. Proceedings of The International Conference on

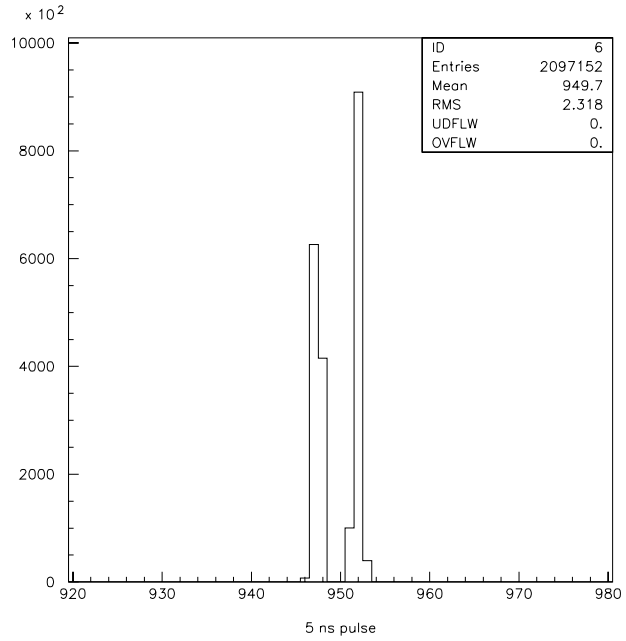

Figure 24: Double edge resolution of a $5\ ns$ wide pulse

Electronic for Particle Physics - LeCroy Research Systems, Chestnut Ridge, May 1995.

8. IEEE Standard VHDL Language Reference Manual, IEEE Std.1076-1987.

9. M. Passaseo, E. Petrolo, R. Vari, S. Veneziano; 32 channel TDC VME board - User Manual. KLOE MEMO 105/97.

The Trigger and Data Acquisition System of the KLOE Experiment [†]

Abstract

Due to the high peak luminosity of the DA Φ NE accelerator (10^{33} $cm^{-2}s^{-1}$) event and data rates at KLOE are higher than in any other e^+e^- collider experiment. The developed 2 level trigger achieves an efficiency larger than 99% for all events relevant to investigate CP violation. The data acquisition system can handle data rates of 50 Mbytes/s using custom designed bus systems and high performance networking techniques.

1 Introduction

KLOE (K-LOng Experiment) is one of three experiments under construction for the Φ-factory DA Φ NE in Frascati. The main goal of KLOE is to investigate CP violation in the neutral kaon system. Particularly a measurement of the ratio Re(ϵ'/ϵ)with a precision of $O(10^{-4})$ is aimed at. In addition a series of interesting interference measurements can be carried out, in order to determine all parameters of the neutral kaon system ([6]- [9]). The detector and physics program is described elsewhere in these proceedings [10] [11] and in [1]- [9].

Stringent conditions for accelerator and experiment are imposed by the aimed precision of the measurements. To achieve sufficiently high statistics, DA Φ NE is designed to run at a peak luminosity of 10^{33} $cm^{-2}s^{-1}$, which corresponds to a Φ-decay rate of 5 kHz. Given the average event size of 5 Kbytes, maximal data rates of 25 Mbytes/s are expected from physics events.

Various background sources at high rates and with event topologies similar to those of physically interesting events make triggering at KLOE a challenging enterprise.

For data acquisition (DAQ) a flexible system has been developed, which allows data rates up to 50 Mbytes/s. If necessary the data throughput can easily be enhanced without changing the existing structure of the system.

2 The Trigger System

2.1 Principle of the KLOE Trigger

The KLOE trigger is a two level system, using information of the electromagnetic calorimeter [10], [2] and the drift chamber [3]. It runs continuously, since the high bunch crossing

[†] *Contributed paper to the V International Conference on Advanced Technology and Particle Physics, Como Italy, October 7-11, 1996*

rate of 370 MHz excludes a trigger decision to be formed between bunch crossings. Trigger signals are synchronised to the DA Φ NE clock before being sent to the Front End Electronics (FEE), to permit offline determination of the specific bunch crossing of a triggered event.

For several physical measurements the efficiencies off all involved Φ decay channels have to be known with a precision of $O(10^{-4})$. In order not to introduce biases in the measurement of the four branching ratios $K_L(K_S) \to \pi^0\pi^0$, $K_L(K_S) \to \pi^+\pi^-$ the corresponding trigger efficiencies must be close to unity. Monte Carlo simulations have shown, that for all events involved in CP violation measurements the efficiencies are larger than 99.5%. The following table shows efficiencies for three important CP-violating $K_{S,L}$ decay channels.

$\Phi \to K_L K_S$	level 1 ϵ (%)	level 2 ϵ (%)
$\to \pi^0\pi^0\pi^0\pi^0$	99.9	99.9
$\to \pi^+\pi^-\pi^+\pi^-$	99.7	99.6
$\to \pi^+\pi^-\pi^0\pi^0$	99.8	99.6

Particles from background events are entering the KLOE detector with a rate of several hundred MHz. Main sources are machine background (beam gas interactions, Touchek effect), cosmic ray muons, and Bhabha scattering. Cosmic ray muons can be tagged without degrading the efficiency for physics events by triggering on events with 2 hits in the out most layer of the barrel calorimeter. The presence of the focusing quadrupoles in the detector volume make Bhabha events in the polar angle range from $3^\circ < \theta < 9^\circ$ (rate: ≈ 300 kHz) and part of the machine background difficult to recognise on trigger level, because particles start to shower in the material of the quadrupoles, leaving a continuous energy spectrum in the calorimeter (figure 25) or a large number of hits in the drift chamber. It follows, that it is not sufficient to trigger on the visible energy of an event, but sensitivity to the number of particles in the detector volume is required.

To achieve a high trigger purity, the following differences between physics and background events are exploited:

- Calorimeter hits of background events are concentrated in the endcaps, since the particles have a low transverse momentum with respect to the beam.
- Background events have drift chamber hits predominantly in the region close to the beam pip, whereas in physics events they are distributed all over the chamber volume (figure 26).
- Background events in general have relatively low multiplicities in the calorimeter and the drift chamber.

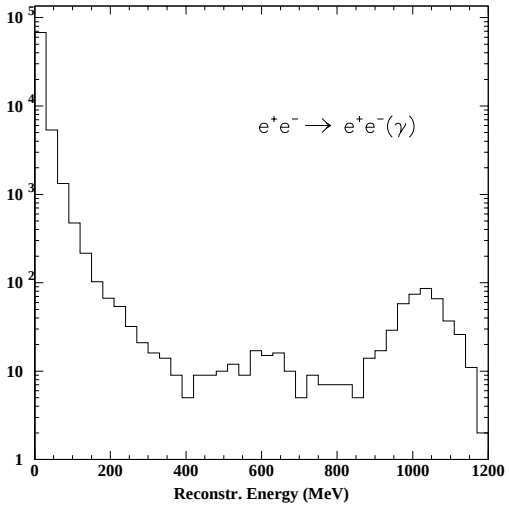

Figure 25: Energy deposit in the entire calorimeter for Bhabha events in the angular range of $1^\circ < \Theta < 179^\circ$.

Table 1 shows Monte Carlo results for trigger rates of the discussed background processes.

Table 1: Monte Carlo results for trigger rates on Φ decays and various background sources.

event type	level 1 rate [kHz]	level 2 rate [kHz]
all Φ	$\sim$5	$\sim$5
Bhabha	7.22	3.10
Machine	1.30	0.98
Cosmic	1.55	1.55
total	10.07	5.53

2.2 Implementation of the Trigger System

The block diagram in figure 27 shows the trigger logic and the trigger conditions foreseen for KLOE.

For triggering purposes the whole granularity of the calorimeter (5000 photo-multipliers) is not needed. The calorimeter is divided into 200 overlapping sections comprising 20 to 30 adjacent photo-multipliers on each readout side of the calorimeter. Analogue signals of

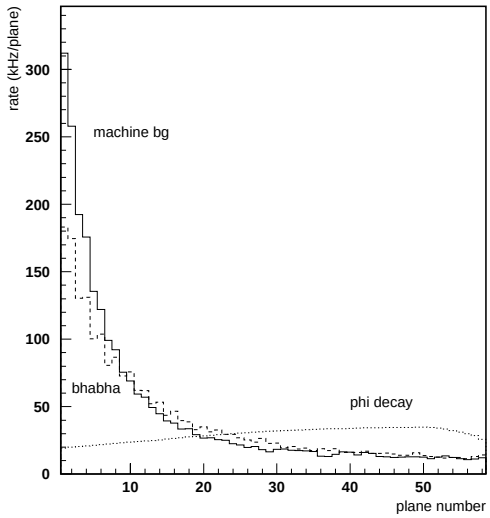

Figure 26: Hit distribution for various event types in the KLOE drift chamber. Planes are ordered from small to large radii.

these sectors are summed for each readout side separately, and are then applied to 2 programmable trigger thresholds. The lower threshold is needed to trigger on small energy deposits by low energetic particles, the higher to form a veto for Bhabha events.

The drift chamber is divided into concentric rings (*"superlayers"*), for which the number of hits in the last 150 ns is counted. Particles from background events with low transverse momentum spiralise in the magnetic field, leaving a large amount of hits in a small number of different superlayers. In order to weigh these particles less, hit counting saturates in each superlayer at values between 2 and 5. Then the total number of hits is formed and compared to the threshold for the first level trigger. Due to the drift time, 150 ns after an interaction only 25% of the hits in an event are available. This information is not sufficient to provide a 99% efficiency for $K_{S,L}$ decays with many charged tracks.

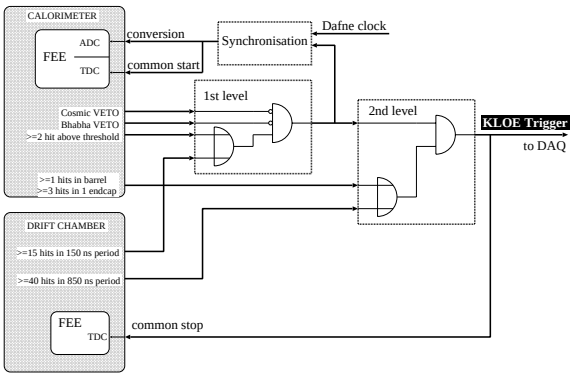

Figure 27: Architecture and conditions of the KLOE trigger system.

Therefore a second trigger level is introduced, which accumulates information of the drift chamber for 850 ns after the first level trigger. In this time more than 80% of the hits have arrived in the chamber, allowing a sufficient discrimination of background and Φ decays.

The final trigger decision will be generated in an crate, the *trigger box*, which to a large extend will be programmable in order to be able to respond quickly to changing trigger requirements.

3 The Data Acquisition System

Figure 28 shows a block diagram of the DAQ architecture. In order to make the DAQ

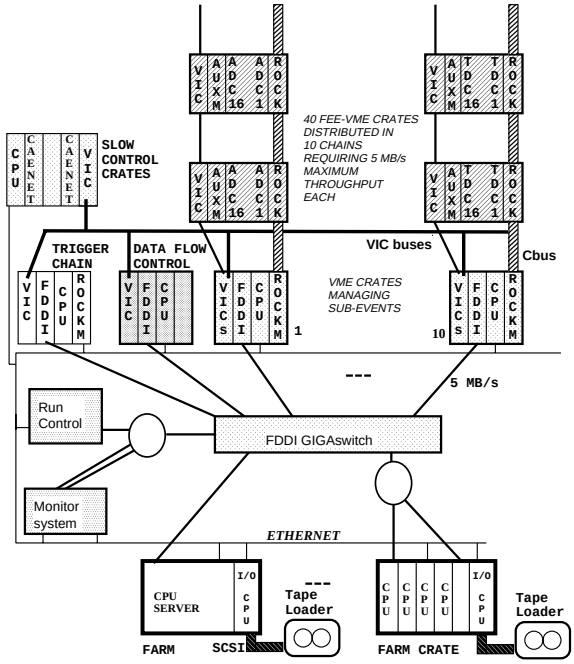

Figure 28: Architecture of the KLOE DAQ system.

system tolerant against peaks in the data rates, and to guarantee a fixed dead time of 2 μs for every given 1st level trigger, every FEE module is given a local buffer, so that its readout need not be synchronised to the actual trigger signal.

The acquisition process can be divided into three different stages. Each FEE crate houses a *Read Out Controller for Kloe* (ROCK), which on a given signal from the Trigger initiates the readout of the crate for a specific event number. The crate readout uses a custom designed bus system (AUX-bus), which has been optimised for the relatively low channel occupancy in KLOE events. The FEE crates are grouped into 10 chains, which all end in dedicated crates housing a chain controller (the ROCK-Manager, ROCKM), and a CPU with an FDDI interface. Each ROCKM is collecting event data from the ROCKs of its chain via the custom designed chain bus (C-bus). The CPUs then send the sub events via FDDI to a switch, from where they are distributed to a farm of powerful processors,

which perform event building, event preprocessing, and finally write events to tape. By maintaining address tables in all CPU-crates, the Run Control system guarantees that all sub events originating from the same event are send to the same processor.

Each C-bus allows data rates up to 5 Mbytes/s resulting in a maximum of 50 Mbytes/s for the whole experiment with 10 chains. If in future higher rates are needed, the system can be upgraded by simply adding new chains. The data throughput of the switch with 3.6 Gbytes/s is largely sufficient for KLOE needs. The final choice for the processor farm will be delayed as long as possible in order to optimise cost effectiveness.

The performance of the AUX-bus and the readout chains has been simulated using the Verilog Hardware Description Language. With the assumptions of 80 words/event for a calorimeter chain and 120 words/event for a drift chamber chain, the readout time for an event results in $\approx 35\ \mu s$, allowing a total trigger rate of 10 kHz.

4 Summary

For KLOE a flexible and conceptually simple two level trigger system has been developed. Trigger decisions base on the number of particles in the calorimeter and a weighted hit sum of the drift chamber. Simulation calculations have shown that the system satisfies all requirements imposed by accelerator configuration, hardware of the detector, and physics needs. The total rate of the trigger at peak luminosity is $\approx 10\ \mathrm{kHz}$ with a signal to background ratio of 1:1. The efficiencies for all important $\mathrm{K}_{S,L}$ decay channels are higher than 99.5%, allowing to control their uncertainties to a level of $O(10^{-4})$.

The data acquisition system handles a data rate of 50 Mbytes/s. It uses custom designed bus systems optimised for the low channel occupancy in KLOE. By simply adding more readout chains to the system, its performance can be increased without modifying the existing structure.

References

1. The KLOE Collaboration, A general Purpose detector for DA Φ NE , *LNF*-92/019 (1992).
2. The KLOE Collaboration, The KLOE Detector, Technical Proposal, *LNF*-93/002 (1993).
3. The KLOE Collaboration, The KLOE Central Drift Chamber, Addendum to the Technical Proposal, *LNF*-94/028 (1994).
4. The KLOE Collaboration, The KLOE Data Acquisition System, Addendum to the Technical Proposal, *LNF*-95/014 (1995).
5. The KLOE Collaboration, The KLOE Trigger System, Addendum to the Technical, *LNF*-96/043 (1996).

6. various articles in *Proc. of the Workshop on physics and Detectors for DA Φ NE* , ed. G. Pancheri, Frascati (1991).

7. various articles in *Proc. of The DA Φ NE Physics Handbook*, ed. L. Maiani, G. Pancheri, N. Paver, Frascati (1992).

8. various articles in *Proc. of The second DA Φ NE Physics Handbook*, ed. L. Maiani, G. Pancheri, N. Paver, Frascati (1995).

9. various articles in *Proc. of the Workshop on Physics and Detectors for DA Φ NE '95*, ed. R. Baldini, F. Bossi, G. Capon, G. Pancheri, Frascati (1996).

10. Contribution of M. Antonelli in these proceedings.

11. Contribution of M. Napolitano in these proceedings.

Message System and Data Transmission in the KLOE Data Acquisition System †

Abstract

Since the KLOE Data Acquisition System is distributed in a multi-platform UNIX environment, event data, status information and run control commands have to be transmitted over the network. Different protocols are used for the different types of information transfers in order to achieve the best performances in speed and reliability. The communication methods used in the KLOE DAQ and the results of some performance tests will be presented.

1 A short Introduction to the KLOE DAQ Architecture

The KLOE experiment [1], being built at the new Φ factory DAΦNE in Frascati, is planned to run at the beginning of 1998; it will perform CP-violation studies at sensitivity of the order of 10^{-4}. The data rate from the detector at full luminosity is estimated to 10^4 events/s, corresponding to a total throughput of 50 MBytes/s. With these requirements, fast electronics, fast data transmission and efficient on-line software had to be designed for KLOE Data Acquisition.

The KLOE DAQ system uses a FDDI GIGAswitch to connect 10 readout chains to 10 farms of processors. In the readout chains - through custom modules and buses - the data coming from the detector pass a two level concentration; a commercial VME-CPU board in each chain is in charge of collecting packets of sub-events and sending them through the switch to a given processor in a farm. The packets of sub-events related to the same trigger number have to be sent to the same farm, where the complete event is build. The correspondence between data packets and event building processors is dynamically managed by the Data Flow Control (DFC), that optimises the traffic on the switch ports and the load of the farm processors.

In the described architecture network functionalities are crucial for the system operation. While standard TCP/IP is used for data transmission, network management and "inter-node" communication (from now on we will call "node" each DAQ processor) are implemented using the Simple Network Management Protocol . The standard SNMP [2] is based on reliable UDP and is widely used to manage network devices. Information about the managed objects is represented as tree of variables in a Manager Information Base (MIB), where variables can be retrieved or set by a SNMP daemon running on the remote device. Extensions of the standard MIB allow to manage private information.

† *Contributed paper to CHEP'97, Berlin Germany, April 7-11, 1997*

2 The Message System

The commands issued by the Run Control and the requests by monitoring and debugging tasks are distributed in the system in the form of messages, with command acknowledge mechanisms. All the programs taking part to the KLOE DAQ comply with a common skeleton, that implements the message system and the storage of relevant information in a shared memory.

Inside a single node the inter-process communication is implemented, according to the UNIDAQ [3] model, with standard UNIX facilities: each process has a message queue, where commands are queued by the sender process, and a signal is also sent to inform the receiver of command arrival. The message queue number is hold in a shared memory, where relevant parameters for each process running on the node are registered.

To carry out communication between remote nodes, a "command server" implemented as a SNMP daemon runs on each node; the standard MIB has been extended to introduce the KLOE subtree, where the command server maps all the variables held in the local shared memory. This makes information about each local process accessible from the network.

Let's have a closer look to the way of sending commands to remote processes and to get two levels of acknowledgement. The sender transmits its communication request to the command server of the node where the destination process is running, locating in this way the MIB variables corresponding to the destination process.

The message is forwarded to the local process by the command server, with the procedure previously described for communication inside the single node.
The first level of acknowledgement means that the message has been received by the process: it is obtained when the destination process itself writes the received command string in a variable stored in shared memory. In fact the sender process continues querying this value to the command server, until it corresponds to the sent message. Then the sender begins to require to the command server the second level of acknowledgement, which is got when the destination process completes the execution of the command and updates a state value in the shared memory to "success" or "error". Opportune timeouts are set to assure the communication termination in case of faults.

A command syntax has been defined that allows the Run Control to send a message to a list of destinations, in a sequential or parallel mode, depending if the execution of the command by the different processes in the list is correlated or independent. In the first case the command is sent to the next process in the list only when the previous one has acknowledged a successful execution. In the case of parallel mode, the message is dispatched to all the destinations in the list, command execution takes place in parallel and a global acknowledge is obtained when all processes have completed their executions.

Performance measurements have shown that less then 30 ms are needed to send a remote command and get all the related acknowledgements, while 1.2 ms is needed if the command is sent locally (on a HP 900/735 processor).

3 The Data Transmission

The flow of event data in our system, as described in the introduction, is shown with more details in Fig. 1. In the second level of the readout chain, the "collector" process reads from a FIFO the sub-event data coming from the electronic modules and builds packets containing a fixed number of sub-events. These streams are distributed in a multiple circular buffer, where each buffer has a defined destination assigned by the DFC [4].

The circular buffer allows to pass event data between two processes with very simple mechanisms and avoids unnecessary data copies; in particular a multiple circular buffer behaves as a parallel pipe between processes. The "sender" is the level-2 process in charge of opening the TCP/IP connections with the destination farm nodes, extracting the sub-event streams from the parallel pipe and sending the packets in parallel through the FDDI GIGAswitch.

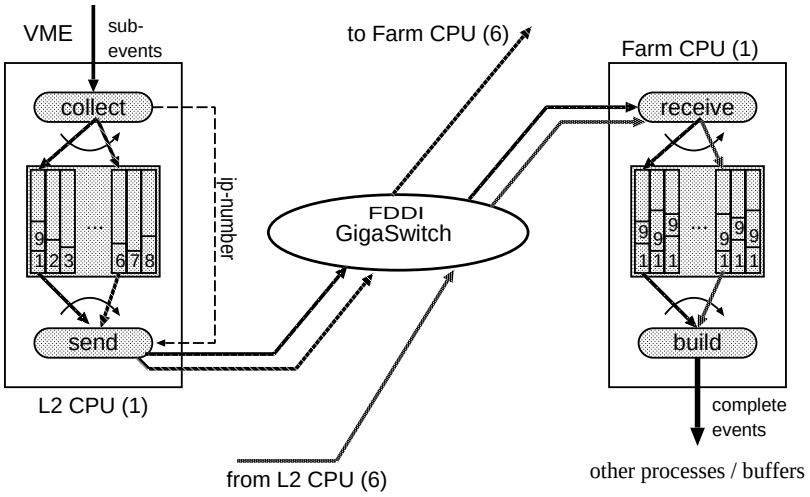

Figure 29: Event Data Flow in the KLOE DAQ

On each farm node a "receiver" process runs, that accepts the TCP/IP connections from the senders and gets sub-event packets in parallel, filling another parallel pipe, from which the process that performs event building takes its input.

The described data transmission model has been tested in different configurations using 10 processors connected to the FDDI GIGAswitch to verify the performances of TCP/IP event transfer, the send/receive software and the switch behaviour under load. The test environment was very heterogeneous (HP/HP-UX, Alpha/OSF1, PowerPC/LynxOS) which represent a bad case for TCP/IP communication.
Only one readout chain was available, so collectors producing random sub-events have been used for the tests with N senders and N receivers. With an estimated event size of 5 KBytes, packing 100 sub-events per stream, the average length per chain is simulated to be 50 KBytes. Using optimised TCP/IP parameters in a 4 (senders) $\times$ 4 (receivers)

configuration, a throughput of ~ 6.8 MBytes/s per each receiver was achieved which is compatible with our requirements. Performing the same test in 1×1 and 1×8 configurations, we verified that N $\times$ N configuration does not put additional load on the system compared to 1×1 and that 1×8 slightly increases the throughput.

References

1. The KLOE collaboration, *KLOE, a general purpose detector for DAΦNE*, **LNF**-92/019 (1992);

2. See Documentation list on *The Simple Times*, **Vol.4, N.1**, January 1996;

3. R.Ball (ed.), *UNIDAQ documentation Set V2.2*, **SDC-93-573**;

4. E.Pasqualucci et al. *Using SNMP implementing Data Flow and Run Controls in the KLOE experiment*, **DAQ96 Workshop**, Osaka November 1996.

Readout optimization for the KLOE QCAL tile calorimeter †

Abstract

A tile calorimeter (QCAL) has been designed for the KLOE experiment. Optimization studies have been conducted by testing the coupling between different types of scintillators and WLS fibers. Results on light yield, attenuation length of fibers and time resolution are presented.

The KLOE experiment [1)] aims at the measurement of R(ε'/ε) with a precision better than 10^{-4}. In order to reduce the signal contamination due to $K_L \rightarrow \pi^0\pi^0\pi^0$ decays, a special electromagnetic calorimeter (QCAL) surrounding the focalization quadrupoles has been designed.

The QCAL(fig 30) is to be placed inside the inner cylinder of the tracking chamber, and must be supported together with the quadrupoles and the beam pipe, thus its weight cannot exceed 350 kg on each arm, and its radial thickness must be smaller than 5.5 cm. Since the QCAL has to act as a veto its capability to detect low-energy photons ($\sim$ 25 MeV) is particularly relevant, while energy resolution is not a major concern. TOF and longitudinal position information is also required.

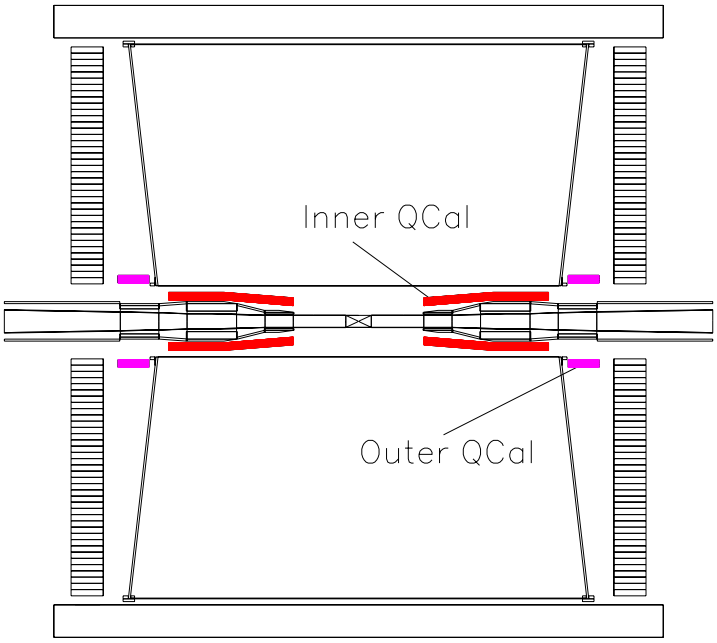

Figure 30: The KLOE detector, in particular the QCAL position is shown.

A Pb-scintillator tile calorimeter with WLS fiber readout has been chosen, due to its high light yield, and to the simplicity of construction. Each QCAL is divided into 12

† *Contributed paper to the VII Pisa Meeting on Advanced Detectors, Elba Italy, May 25-31, 1997*

azimuthal sectors (fig 31) made of 1.9 mm thick lead layers alternating with 1 mm thick scintillator tiles. The radial thickness is about 5.5 X_0. The tiles (60 in a sector) are read out by 1 mm diameter WLS fibers about 2.5 m long, the same fibers reading 2 non-adjacent sectors. Shower TOF and Z position are obtained by measuring the time difference between the signal at both ends. MonteCarlo simulation has shown that the fraction of $K_L \to \pi^0\pi^0\pi^0$ events in which only 4 photons are detected is reduced by the QCAL from $(68.6 \pm 2.8) \times 10^{-4}$ to $(7.2 \pm 0.6) \times 10^{-4}$.

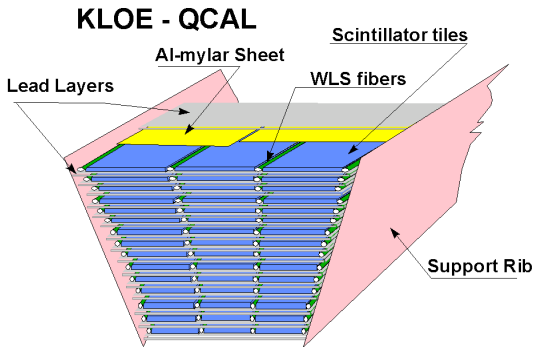

Figure 31: A QCAL module: the lead and scintillator tiles and the WLS fibers are clearly visibile.

The light yield has been measured for different combinations of scintillators and WLS fibers. Electrons from a β source have been directed onto a $10 \times 2\mathrm{cm}^2$ scintillator rectangular tile 1 mm thick, the short side being coupled to a photomultiplier used as trigger. The 1 mm diameter fiber is placed along the tile. Al mylar is used to wrap together the scintillator and the fiber. A second photomultiplier is used to read the light signal from the fiber. Figure fig 32 shows the light yiels (in p.e.) versus the fiber length for different WLS fibers using a BICRON BC-408 scintillator. Other types tested were BC-404 and Pol.Hi.Tech scintillators but they gave inferior results. As a result, it was decided to employ Kuraray Y11-200 multi-clad fibers together with Bicron BC-408 scintillator. Using the measured light yield in the MC simulation of the full QCAL results in about 0.5 p.e. expected per incoming MeV.

A similar setup, with 2.5 m fibers placed on both sides of the tiles and read out at both ends, has been used to measure the TOF resolution (1.45 ns). In this setup a MIP released the same amount of light expected by a 20 MeV photon. As a consequence the expected time resolution for the QCAL is $\sigma = 200\,\mathrm{ps}/\sqrt{E(\mathrm{GeV})}$

In conclusion a QCAL has been designed to reduce in the signal contamination in the KLOE experiment. Suitable WLS fibers and scintillators have been identified, and the chosen setup is capable to measure TOF and longitudinal position.

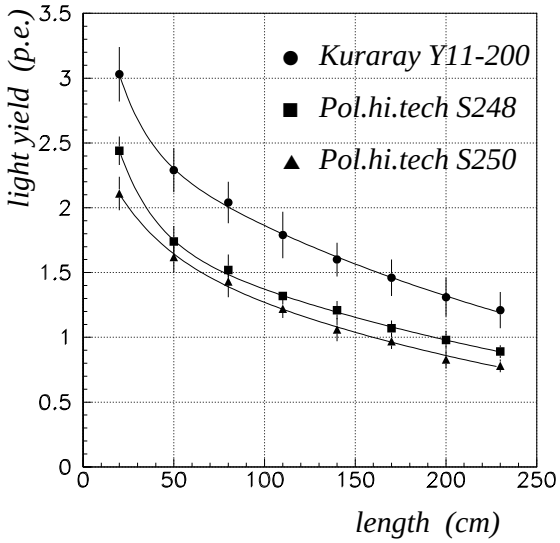

Figure 32: Attenuation length for several fibers: light yield vs. fiber length is shown, data are fitted with 2 exponentials.

References

1. “The KLOE Detector, Technical Proposal”, The KLOE collaboration, Report LNF-93/002, 21 January 1993